Available online at www.sciencedirect.com
SCIENCE DIRECT®
ELSEVIER
Progress in Energy and Combustion Science 30 (2004) 679–717
PROGRESS IN ENERGY AND COMBUSTION SCIENCE
www.elsevier.com/locate/pecs

Coal conversion submodels for design applications at elevated pressures. Part II. Char gasification

Gui-Su Liu, Stephen Niksa*

Niksa Energy Associates, 1745 Terrace Drive, Belmont, CA 94002, USA

Received 2 January 2004; accepted 13 August 2004
Available online 27 September 2004

Abstract

This paper surveys the database on char gasification at elevated pressures, first, to identify the tendencies that are essential to rational design of coal utilization technology, and second, to validate a gasification mechanism for quantitative design calculations. Four hundred and fifty-three independent tests with 28 different coals characterized pressures from 0.02 to 3.0 MPa, CO_2 and steam mole percentages from 0 to 100%, CO and H_2 levels to 50%, gas temperatures from 800 to 1500 °C, and most of coal rank spectrum. Only a handful of cases characterized inhibition by CO and H_2, and only a single dataset represented the complex mixtures of H_2O, CO_2, CO, and H_2 that arise in practical applications. With uniform gas composition, gasification rates increase for progressively higher pressures, especially at lower pressures. Whereas the pressure effect saturates at the higher pressures with bituminous chars, no saturation is evident with low-rank chars. With fixed partial pressures of the gasification agents, the pressure effect is much weaker. Gasification rates increase for progressively higher gas temperatures. In general, gasification rates diminish for coals of progressively higher rank, but the data exhibit this tendency only for ranks of hv bituminous and higher.

These tendencies are interpreted with CBK/G, a comprehensive gasification mechanism based on the Carbon Burnout Kinetics Model. CBK/G incorporates three surface reactions for char oxidation plus four reactions for gasification by CO_2, H_2O, CO and H_2. Based on a one-point calibration of rate parameters for each coal in the database, CBK/G predicted extents of char conversion within ± 11.4 daf wt% and gasification rates within $\pm 22.7\%$. The predicted pressure, temperature, and concentration dependencies and the predicted inhibiting effects of CO and H_2 were generally confirmed in the data evaluations. The combination of the annealing mechanism and the random pore model imparts the correct form to the predicted rate reductions with conversion. CBK/G in conjunction with equilibrated gas compositions accurately described the lone dataset on complex mixtures with all the most important gasification agents, but many more such datasets are needed for stringent model evaluations.

Practical implications are illustrated with single-particle simulations of various coals, and a 1D gasifier simulation for realistic O_2 and steam stoichiometries. The rank dependence of gasification rates is the determining factor for predicted extents of char conversion at the gasifier outlet. But soot gasification kinetics will determine the unburned carbon emissions for all but the highest rank fuels. Only gasification kinetics for gas mixtures with widely variable levels of H_2O, H_2, and CO are directly relevant to gasifier performance evaluations.

Keywords: Coal; Pressure; Char; Gasification; Gasifier; Modeling; Simulation

Abbreviations: CBK, carbon burnout kinetics model; CFD, computational fluid dynamics; daf, dry-ash-free basis; EFR, entrained flow reactor; FlB, fluidized bed reactor; FxB, fixed bed reactor; IGCC, integrated gasification combined cycle; PDTF, pressurized drop tube furnace; p.f., pulverized fuel; PTGA, pressurized thermogravimetric analyzer; SNOR, single *n*th-order reaction; SSE, sum-of-squares error estimate; SR, stoichiometric ratio; WMR, electrically heated wire-mesh reactor.

* Corresponding author. Tel.: +1 650 654 3182; fax: +1 650 654 3179.
E-mail address: neasteve@pacbell.net (S. Niksa).

0360-1285/$ - see front matter © 2004 Elsevier Ltd. All rights reserved.
doi:10.1016/j.pecs.2004.08.001

Contents

Nomenclature

a_i	polynomial coefficients ($i=0$–5)
A_i	pre-exponential factor (s^{-1} or $atm^{-1}\,s^{-1}$) of reaction i
A_i'	pre-exponential factor (s^{-1} or $atm^{-1}\,s^{-1}$) of reaction i'
C	gas mole concentration (mol/m^3)
C_{daf}	DAF carbon content in coal
d_P	particle diameter (μm)
D	effective diffusivity (m^2/s)
E_i	activation energy of reaction i (kJ/mol)
E_i'	activation energy of reaction i' (kJ/mol)
f_{RPM}	rate factor accounting for random pore model
k_i	reaction rate constant of reaction i (s^{-1} or $atm^{-1}\,s^{-1}$)
k_i'	reaction rate constant of reaction i' (s^{-1} or $atm^{-1}\,s^{-1}$)
K_i	rate constant ($i=$1a, 1b, 2, 3, CO or H_2)
m	particle mass (kg)
n	reaction order
n_s	number of total data records
n_F	number of factors
P	pressure (atm)
p_i^p	predicted value of record i
p_i^o	measured value of record i
$\bar{P}$	mean pressure (atm)
q	depletion flux ($kg\,m^{-2}\,s^{-1}$)
R	gas constant (kJ/mol)
R_i	rate of reaction i (s^{-1})
R_i^0	surface reaction rate not subject to annealing and physical evolution (s^{-1})
S	internal surface area per volume (m^2/m^3)
t	time (s)
T	particle temperature (K)
X	carbon conversion (%)
α	exponent in $\rho/\rho_0=(m/m_0)^\alpha$
β	$d_P S\eta/2$
γ	k_7/k_5
η	effectiveness factor
θ	fractional surface coverage by the C(O) complex
ϑ	coefficient for annealing and physical evolution effects in the global gasification rate law
ρ	particle density (kg/m^3)
ν	stoichiometric coefficient of a gas–solid reaction
ϕ	Thiele modulus
ψ_0	structural parameter in the random pore model
ϖ	collection of various rates in Eqs. (22a) and (22b)

Subscripts

0	reference or initial environment
∞	ambient environment
C	carbon
CH_4	methane
CO	carbon monoxide
CO_2	carbon dioxide
C-Com	char combustion
C-Gas	char gasification
C-CO_2	char gasification by CO_2
C-H_2O	char gasification by H_2O
C-H_2	char gasification by H_2
H_2	hydrogen
H_2O	steam
HT	heat treatment
i	ith reaction
S	surface

1. Introduction

Gasification converts carbonaceous pulverized fuels (p.f.) into synthesis gas, a mixture of CO and H_2 that is a raw material for chemicals as well as a fuel for producing electricity. Gasification has the best fuel flexibility of any of the advanced technologies for power production, and current technology has already operated well with biomass and other low-value feedstocks, and with high-ash residues. Integrated gasification combined-cycle (IGCC) processes are arguably the cleanest, most efficient means of producing electricity from coal. Entrained coal gasifiers have typically operated at 2.5–3.0 MPa, although pressures must be raised to 6.0–8.0 MPa to couple in some CO_2 sequestration schemes. They run at temperatures to 2000 °C and overall stoichiometric ratios (SR) of about 0.8. Fluidized bed gasifiers operate at similar pressures and more moderate temperatures with SR values as low as 0.7. Different gasification technologies are being developed in many of the major industrialized nations, including Japan which imports coals from all the major coal producing regions worldwide. Consequently, they will be fed with coals representing the entire range of coal quality, from lignites to subbituminous to high volatile (hv) bituminous to low volatility coals.

Today, any major technology development effort is almost always supported by computational fluid dynamics (CFD) and/or other design calculation schemes. Such massive calculations are organized into submodels for each of the essential physicochemical stages. There are independent submodels for fluid dynamics, particle dynamics, heat transfer, coal conversion chemistry, and chemistry in the gas phase. We will only consider reaction mechanisms that are essential elements of a submodel for

coal conversion chemistry at elevated pressures, particularly the following three steps:

(1) The partitioning of the coal feed into volatiles and char is crucial because volatiles are subsequently converted into ultimate products on much shorter time scales than char. The reaction mechanism responsible for the partitioning is called 'devolatilization'. It governs the stabilities of flames on the fuel injectors and also affects temperature profiles and all the major emissions. Devolatilization behavior is widely variable, even among different samples of the same type—or 'rank'—of coal. Devolatilization kinetics are needed in simulations, but the total volatiles yield is the crucial characteristic. The O_2 requirement for volatiles combustion and the associated heat release are also important. Volatiles species compositions are generally ignored in design calculations.
(2) Char oxidation must be described because, even in gasifiers, O_2 is injected in a first stage to raise the process operating temperature into the target range. A suitable reaction mechanism must automatically adjust the limiting rate process to correctly predict the burning rate, beginning with the intrinsic chemical kinetics at low temperatures, then O_2 transport within the char at moderate temperatures, then O_2 transport from the bulk gas flow to the external char surface at the highest temperatures. Also, the intrinsic kinetics must also depict the substantial differences among the reactivities of chars from diverse coal types, as well as the loss of reactivity by annealing at temperatures above 1000 °C. Additional factors reduce burning rates during the latest stages of burnout, such as the size reductions that lower particle temperatures, thereby re-instituting chemical kinetic control and, in some special cases, the hindered transport through ash layers [1].
(3) The residual char from the first stage must be completely converted into ultimate products, simply because fuel costs are the major component of process operating costs. When O_2 is not present, chars are gasified by the combined chemistry of CO_2, H_2O, CO, and H_2 in the process stream. Differences in char reactivity are thought to be even more important in gasification than in oxidation, because the reaction times are so slow that the gasification agents can penetrate deeper into the chars' internal pore structures. A more significant difference is that even though steam is injected or raised from water in a feed slurry, the concentrations of the gasification agents are mostly determined by chemistry in the gas phase that partially oxidizes and reforms the primary volatiles.

Part I of this review [2] covered devolatilization and char oxidation. Char reactivities for other gasification agents (CO_2, H_2O, CO, and H_2) are surveyed here in Part II. These same topics were recently discussed in PECS by Wall et al. [3], but with the objectives of thoroughly reviewing the experimental work and surveying some of the major modeling approaches. Our papers are complementary in the sense that we emphasize reaction mechanisms, and use test results primarily to evaluate the mechanistic models.

Our aim is to validate a reaction mechanism for char gasification that can predict the extents of conversion and gasification rates from any coal for heating rates to 10^5 °C/s, temperatures from 800 to 2000 °C, and pressures to 3 MPa. The complete range of CO_2 and H_2O concentrations must be depicted, and also CO and H_2 levels up to 50%. The ultimate goal is to establish a new benchmark for the quantitative accuracy of predictions for char gasification reactivity by evaluating the model predictions against all the available test results in the English literature that specified the required input for the simulations. Once validated, the reaction mechanism becomes a means to manage gaps in the current laboratory database, especially for the complex mixtures found in commercial gasifiers.

Our research strategy is regarded as classical in many branches of engineering science, but is unique in this area: first, all the datasets on char gasification at elevated pressure in the English literature were qualified for their suitability for model validations. Then selected datasets from various sources were combined to clearly illustrate the tendencies for all the important operating conditions, including coal quality. Then the predictions from the reaction mechanisms were evaluated with each dataset, and the discrepancies were compiled into statistics for the 'best' representation of the entire database. Although model parameters may have been tuned at various stages in the data evaluations, all model predictions in this paper are based on the ultimate sets of parameter estimation algorithms for the gasification mechanism.

At the outset, it is worth noting that several essential mechanisms for detailed process simulations involving char gasification are omitted from most of the discussion, particularly the connections among gasification rates and chemistry in the gas phase and on soot. These issues are illustrated in the application case studies, but never resolved at a deep technical level. Similarly, all the necessary transport and chemical mechanisms to describe char gasification at the level of individual particles are considered, but subsequent shifting of the primary gasification products by gas phase chemistry is omitted. Essential aspects of single-particle gasification in fluidized systems are also omitted, including the fragmentation and comminution that are usually primary mechanisms for mass loss in bubbling fluidized beds.

This paper is organized the same way that the research was conducted, except for the addition of a section on design applications after the model validation section.

2. Database on pressurized coal gasification

By the time the coal suspension leaves the devolatilization and char oxidation stages of a coal gasifier, all the O_2 has been consumed, and steam and CO_2 become the primary agents for gasification. The gas phase also contains H_2 and CO. Hydrogen directly inhibits steam gasification, whereas CO inhibits steam gasification but promotes CO_2 gasification indirectly through the homogeneous chemistry of water-gas shifting. The process stream cools throughout gasification because the heterogeneous chemistry is endothermic. Catalysis by dispersed inorganic species, especially Ca and K, is important in low-rank coal chars, which masks any continuous rank dependence because cation loadings do not change continuously with rank. Compared to the chemistry that underlies devolatilization and combustion, gasification mechanisms are thought to be relatively insensitive to coal rank for ranks of bituminous and higher.

2.1. Prerequisites for data on pressurized char gasification

Gasification is much easier to monitor than char oxidation for two reasons. First, gasification rates at high temperatures in steam and CO_2 are much slower than char oxidation rates. Second, the absence of strong exothermic reactions dramatically simplifies temperature control. In fact, char and gas temperatures are nearly the same, provided that the suspension loadings are low enough to avoid bulk gas cooling. Hence, the coupling among transport and chemical reaction mechanisms is much weaker for gasification than combustion. Diffusional resistances will often come into play at the highest gasifier temperatures, but without coupling to the temperature history.

Due to the weak mechanistic coupling to the transport mechanisms, there is no strong motivation to use entrained flow systems to monitor gasification histories. Provided that the test configuration is simple enough to assign the transport coefficients within useful quantitative tolerances, tests in fixed bed reactors do provide data that are relevant to entrained coal gasification.

From the standpoint of evaluating a complex gasification mechanism for applications in entrained-flow and/or fluidized bed gasification, the chars need to be prepared at relatively fast heating rates. Although data on this aspect have only begun to appear very recently [4–8], preliminary indications are that the exposure temperature and the heating rate exert independent influences (although most systems that impose fast heating rates operate at high temperatures). The impact of char preparation pressure on subsequent gasification reactivity is also just now beginning to be characterized [3], but it seems to be very weak. To characterize the extent of gasification, the conversion assigned from the mass fraction of carbonaceous material remaining (on a dry-ash-free (daf) basis of the residual char from devolatilization) is the most useful conversion index. Supplemental characterization of a char's physical structure is also helpful, particularly if surface areas are monitored over a wide range of conversion.

The gas composition for model evaluations should be highly variable, including simplified systems with only steam and only CO_2, as well cases with steam plus H_2, steam plus CO_2, and steam, CO_2, H_2 and CO. The value in a series of cases with progressively more complex gas compositions is that specific terms in the rate expressions can be evaluated more stringently in the simpler cases before the complete rate law is validated with the most complex cases.

More formally, the following testing features are required if a dataset can be used to evaluate a comprehensive gasification rate model:

(1) *Coal properties*. As-yet unknown factors determine the rank dependence of the initial char gasification reactivity. In general, the strong impact of mineral catalysis obscures the true rank dependence, which is thought to be weak for the coals of greatest commercial interest. Initial bulk density and initial char particle size are also required.
(2) *Pressure*. Usually a uniform test pressure will be specified.
(3) *Partial pressures of participating gases*. Uniform levels of steam, CO_2, H_2, and CO across a wide domain of gas compositions must be represented.
(4) *Thermal history*. Sufficient information must be available to assign the temperature of the sample throughout an entire test, which is particularly straightforward if the suspension loading in entrained systems is low or if the space velocity in fixed bed systems is high.

A fair assessment of the current status of gasification rate modeling would be that the gasification rate of any char across the entire domain of gasification conditions can be accurately represented with reported rate laws, given data on the rate and surface area versus conversion. However, some modeling parameters cannot be predicted within useful quantitative tolerances. There is an imperative to try to identify useful factors that can capture the distinctive gasification behavior of the chars from diverse coal samples. This advance will probably require specific test data on every char that is simulated with the model, and the specifications on the required measurements remain to be defined.

2.2. Database for pressurized coal and char gasification

A database on pressurized coal gasification that satisfies the above prerequisites appears in Table 1, which lists the performing organization, country, literature citations, and the reactor type. Among the 18 selected datasets, 14 were obtained at universities and the rest came from private or not-for-profit research institutions. Several additional datasets had to be excluded due to omissions of necessary information. For example, in the studies by Li and Sun [27]

Table 1
Sources of data on pressurized coal gasification

Organization	Country Code	References	Reactor
Imperial College	UK	[9]	WMR
Imperial College	UK	[10]	WMR
Imperial College	UK	[11]	WMR
Imperial College	UK	[12]	WMR
Imperial College	UK	[13]	WMR
Imperial College	UK	[14]	WMR
University of Amsterdam	NTH	[15]	PDTF
West Virginia University	USA	[16]	PTGA
Eindoven University of Technology	NTH	[17]	WMR
Åbo Akademi University	FIN	[18]	PTGA
East China University of Chemical Technology	CHN	[19]	PTGA
East China University of Chemical Technology	CHN	[20]	FxB
Institute of Gas Technology	USA	[21]	PTGA
University of Tokyo	JPN	[22]	PTGA
CSIC	ESP	[23]	FlB
CRIEPI	JPN	[24]	PDTF
Korea Electric Power Research Institute	KOR	[25]	PDTF
University of Newcastle	AUS	[26]	PTGA

[a]WMR, wire-mesh reactor; PDTF, pressurized drop tube furnace; PTGA, pressurized thermogravimetrical analyzer; FxB, fixed bed reactor; FlB, fluidized bed reactor.

and Li and Xiao [28], the coal analyses were not given. In the study by Abichandani et al. [29], the operating conditions were not completely specified. Mühlen et al. [30] did not describe the test procedures in sufficient detail.

Seven datasets were obtained with wire-mesh reactors (WMRs), three with pressurized drop tube furnaces (PDTFs), six with pressurized thermogravimetric analyzers (PTGAs), and one each with a fluidized bed and a fixed bed reactor. The database represents 28 different coals of rank from lignite through anthracite. All of the datasets have the required proximate and ultimate analyses.

2.2.1. Characteristics

The database comprises 453 independent tests, each representing a specific pressure, the mole fractions of CO_2, steam, CO, and H_2, gas temperature, coal properties and particle size. The ranges of the test conditions are collected in Table 2, along with a typical value for each operating condition. Pressure was varied from 0.02 to 3.0 MPa, with a typical pressure of 1.0 MPa. This pressure range covers the range for most advanced coal processing technologies, except for CO_2 sequestration processes operated at 6–8 MPa, and the coverage of the pressure domain is uniformly fine. The mole fractions of CO_2 and steam were varied from 0 to 100%, with a typical value of 100% for each. CO and H_2 mole fractions were varied to about 50%. Gas temperature ranged from 800 to 1500 °C, spanning the typical ranges in applications of both fluidized bed and entrained flow gasifiers. Particle size ranged from 50 to 800 μm.

Table 2
Domain of test conditions

Operating condition	Range	Typical value
Pressure (MPa)	0.02–3.0	1.0
CO_2 (mol%)	0–100	100
Steam (mol%)	0–100	100
CO (mol%)	0–46	0
H_2 (mol%)	0–50	0
Gas temperature (°C)	800–1500	1000
Particle size (μm)	50–725	150

2.2.2. Coal quality

The database represents 28 coal samples ranging from lignite to anthracite, or virtually the entire coal rank spectrum. The range of coal quality is illustrated in two ways in Fig. 1. The upper panel is a coalification diagram, which plots the atomic H/C ratio versus the atomic O/C ratio. Data on a coalification diagram generate the coalification band, which is a banded exponential saturation curve emanating from the origin toward higher O/C values. Anthracites and other low volatility coals lie along the steep trajectory from the origin, whereas high volatile bituminous, subbituminous, and lignites lie on the saturation band because their H/C ratios are similar while the oxygen contents progressively increase across these ranks. The coals tested are concentrated in the bituminous rank; otherwise, there were only a few lignites and a few anthracites.

The plot of the proximate volatile matter contents versus carbon content in the lower panel of Fig. 1 underscores the concentration of bituminous coals in the database, and the generally poor coverage of low and high volatility coals. The poor coverage of low volatility coals and subbituminous needs to be rectified in future testing programs.

2.3. Reported gasification behavior

Measurements to characterize coal gasification kinetics should include particle temperature, particle size, and extents of conversion as a function of residence time. The most commonly reported measurements were either extents of conversion or the gasification rate, which are equally distributed among all tests in the database. Generally, particle temperatures and particle sizes were not continuously monitored. Particle temperatures were assumed to remain at values close to the local gas temperatures. Particle size changes very slowly because gasification is usually mediated by internal pore transport, but only partially.

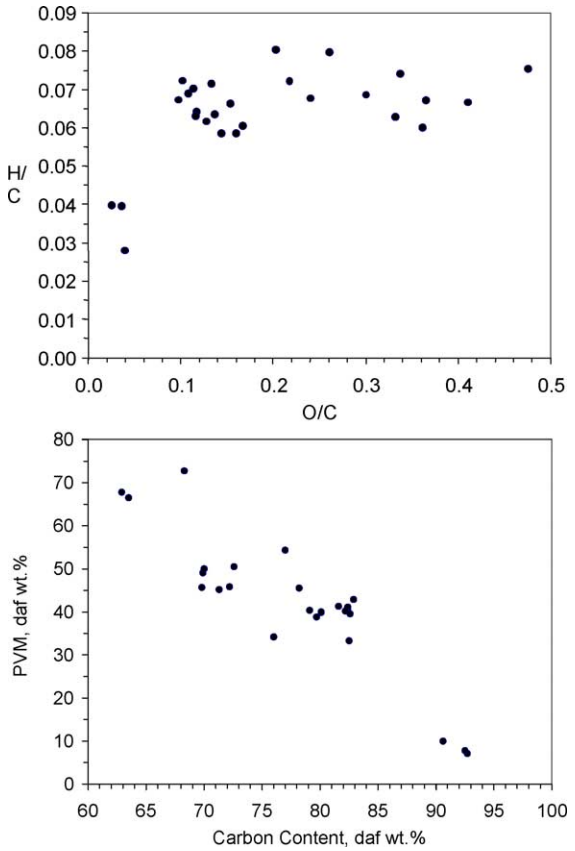

Fig. 1. (Top) Coalification diagram and (bottom) proximate volatile matter contents of coals in NEA's database on pressurized gasification.

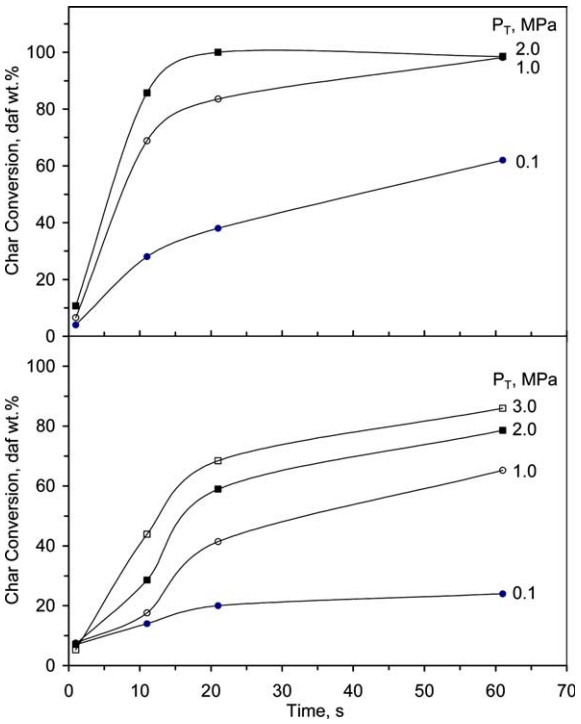

Fig. 2. Char conversion histories for Daw Mill bituminous char gasification under (upper) 80% steam and (lower) 100% CO_2 at 1000 °C and (●) 0.1, (○) 1.0, (■) 2.0 and (□) 3.0 MPa in a WMR [9].

2.3.1. Effect of pressure at constant gas composition

This section illustrates the most important qualitative trends with the gasification characteristics of selected datasets, beginning with the impact of pressure on char conversion and burning rates. Pressure variations can be confusing to unravel because they can affect gasification both directly, by changing reactant partial pressures, and indirectly, by changing transport rates. One testing strategy varies pressure with constant reactant gas compositions, whereby the gas concentrations and partial pressures increase in tandem with pressure. Another varies pressure with fixed partial pressures of all gasification agents. Both strategies are represented in the database among the 14 datasets that evaluated pressure effects, and both are considered here.

Two transient conversion histories of a bituminous char for pressures from 0.1 to 3.0 MPa with fixed gas compositions of 80% steam and 100% CO_2 [9–11] appear in Fig. 2. For steam gasification, the extents of char conversion for all three pressures increase rapidly during the initial 15 s, then much more slowly for further gasification. The gasification rate is significantly accelerated by progressively higher pressures so that, for the longest reaction time, extents of conversion increased from 62 to 98.2 to 98.5 daf wt% at respective pressures of 0.1, 1.0 and 2.0 MPa. The same tendency is apparent in the data for CO_2 gasification. At 61 s, the extents of char conversion were 24, 65.2, 78.6 and 86 daf wt% at pressures of 0.1, 1.0, 2.0 and 3.0 MPa, respectively. The incremental conversion becomes smaller at progressively higher pressures, indicating that this effect saturates.

These datasets also directly compare the gasification rates under CO_2 and steam. Even though the mole percentage of steam is only 80% versus pure CO_2, chars are converted in steam much faster than in CO_2 at pressures from 0.1 to 2.0 MPa. This ranking is consistent with the findings of Mühlen et al. [30] that the steam gasification rate is several times that for CO_2 gasification at the same temperature and partial pressure.

Fig. 3 shows the initial gasification rates of Spanish lignite char measured in a PTGA at 1000 °C under pure CO_2 at pressures from 0.5 to 3.0 MPa [23]. The data clearly exhibit a diminishing sensitivity to pressure variations at progressively higher pressures. At the highest test pressures, the rate approaches an asymptotic value of $1.5–2.0 \times 10^3\ s^{-1}$. These same features are evident in the gasification rates of another lignite char in Fig. 3. The rate of steam gasification was measured at 850 °C in a mixture of steam, H_2 and CO with

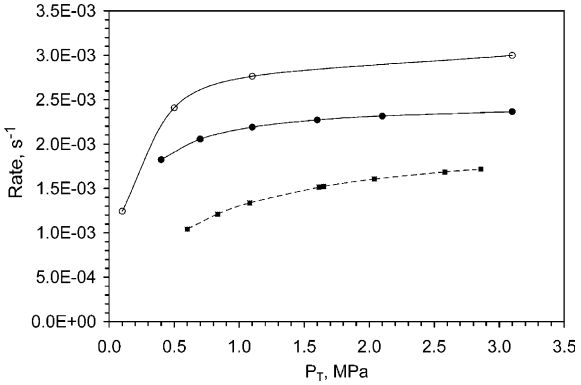

Fig. 3. Initial gasification rates of Xiao Long Tan lignite char at (● and solid curve) 850 °C in 80% steam, 10% H_2, and 10% CO, and at (○ and solid curve) 900 °C and 90% CO_2 and 10% CO [19]; and (■ and dashed curve) of Spanish lignite char at 1000 °C under pure CO_2 [23].

constant mole fractions, whereas the CO_2 gasification rate was measured at 900 °C in uniform mixtures of CO_2 and CO [19]. Again, both the CO_2 and steam gasification rates increase rapidly at pressures below 0.6 MPa, then the enhancement diminishes with further pressure increases. These features were observed under the inhibiting effects of CO and H_2 in two of these datasets.

2.3.2. Pressure variations with variable composition

The initial gasification rates of Newlands char in Fig. 4 were monitored in a PDTF at 1300 °C under constant partial pressures of both steam and CO_2 over a wide pressure range [24]. In 0.05 MPa steam, the gasification rate increased by less than 50% for pressures from 0.2 to 2.0 MPa. But in 0.20 MPa CO_2, the rate was independent of pressure variations. This finding appears to be inconsistent with the tendency in Fig. 5 in the char conversion histories of a subbituminous char in 0.2 MPa CO_2 at pressures from 0.5 to

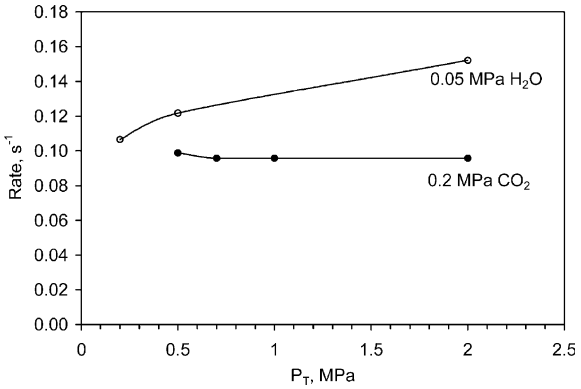

Fig. 4. Gasification rate of Newlands bituminous char at 1300 °C and a (●) CO_2 partial pressure of 0.2 MPa, and (○) steam partial pressure of 0.05 MPa in a PDTF [24].

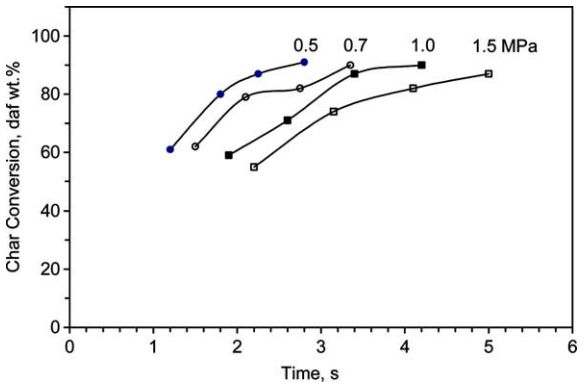

Fig. 5. Char conversion histories for Roto subbituminous char at 1300 °C under 0.2 MPa CO_2 at pressures of (●) 0.5, (○) 0.7, (■) 1.0, and (□) 1.5 MPa in a PDTF [25].

1.5 MPa in another PDTF [25]. The time to achieve a specified extent of conversion increased at progressively higher pressures, implying diminished gasification rates at higher pressures (contrary to both tendencies in Fig. 4). For example, the times needed for 90% char conversion were 2.8, 3.3, 4.2, and 5.5 s at pressures of 0.5, 0.7, 1.0, and 1.5 MPa, respectively.

Notwithstanding, this tendency is in accord with expectations, provided that the gasification reaction is controlled by pore diffusion under these test conditions. Normally a pore diffusion rate is independent of pressure because the pressure dependence in the reactant concentration cancels the inverse proportionality to pressure in the diffusivity. But since the partial pressure of the gasification agent was uniform in these tests, the diffusivity determines the pressure dependence in the transport rate, which would tend to diminish the overall gasification rate at progressively higher pressures, as was observed. All test conditions in Kajitani et al.'s [24] PDTF tests were essentially the same as Ahn et al.'s, except that they tested hv bituminous coal, rather than subbituminous, and the chars were prepared at atmospheric pressure rather than at the elevated test pressure. The insensitivity to pressure in their results would also be consistent with this explanation for Ahn et al.'s results, provided that the lower reactivity of the bituminous char yielded an overall gasification rate that was controlled by the gasification kinetics. Under chemical kinetic control at uniform partial pressures of the gasification agents, there would be no pressure dependence. However, this explanation is inconsistent with the positive pressure dependence for steam gasification in Kajitani et al.'s dataset.

2.3.3. Effect of gas composition

The gasification rates of Newlands char at 1300 °C at 0.5 MPa in Fig. 6 covered broad ranges of steam and CO_2 concentrations. The rate of steam gasification is proportional to the increase in the H_2O mole fraction from 4 to 16%.

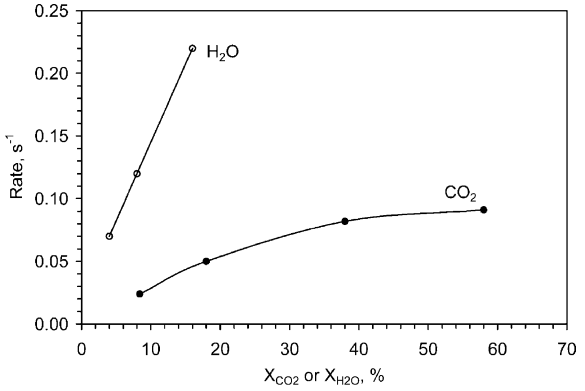

Fig. 6. (●) CO_2 and (○) steam gasification rates for Newlands bituminous char at 1300 °C and 0.5 MPa in a PDTF [24].

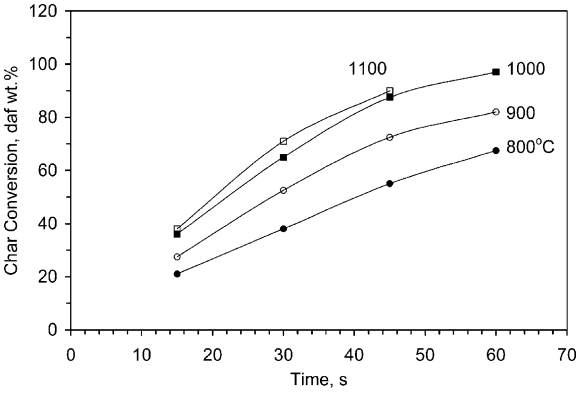

Fig. 7. Char conversion histories of N. Dakota lignite char at (●) 800, (○) 900, (■) 1000, and (□) 1100 °C and 0.78 MPa under 76% steam in a PTGA [16].

Similarly, the CO_2 gasification rate is proportional to the CO_2 level from 8 to 25%. Further increases from 25 to 48% yield almost no additional rate enhancements. At the same mole fractions of the respective gasification agents, the steam gasification rate is about four times faster than rates of CO_2 gasification.

The inhibiting effect of CO on CO_2 gasification is characterized in Table 3 for Spanish lignite char at 1000 °C in a PTGA. In these tests, the partial pressures of both CO_2 and CO increased at progressively higher test pressures, even though the CO_2 mole fraction decreased. The gasification rate, however, generally decreased as the pressure increased, due to inhibition by CO.

2.3.4. Effect of gas temperature

Five datasets characterized the effects of gas temperature variations from 800 to 1500 °C on gasification rates. Fig. 7 shows the conversion histories of a lignite char at 0.78 MPa under 76% steam at temperatures from 800 to 1100 °C [16]. The extents of conversion increased in uniform increments of roughly 15% per 100 °C as temperature was increased from 800 to 1000 °C. The adjustment to 1100 °C, however, increased conversion by only 2.5%, perhaps, because the reaction shifted from zone I to zone II, where pore diffusion is the rate controlling mechanism. A very similar temperature dependence appears in Fig. 8 for a subbituminous char at 1.0 MPa under 20% steam [25], but at significantly hotter temperatures and for much shorter reaction times. The temperature dependence in Fig. 9 for a bituminous char in a WMR at 1.5 MPa under 2.5% CO_2 [17] displays much less uniformity. These conversion histories exponentially approach complete conversion with dramatic reductions in the time constants for progressively hotter temperatures.

Table 3
Gasification rates of Spanish lignite char at 1000 °C and various CO_2 and CO concentrations in a PTGA [23]

P_T (MPa)	CO_2 (%)	CO (%)	Rate (s^{-1})
0.6	88.5	11.5	8.55×10^{-4}
1.1	78.1	21.9	8.79×10^{-4}
1.7	70.7	29.3	8.37×10^{-4}
2.0	63.3	36.7	7.37×10^{-4}
2.6	54.1	45.9	6.08×10^{-4}

2.3.5. Effect of coal rank

In the gasification database, five datasets characterize the impact of coal rank on char gasification. Fig. 10 shows the gasification rate measured at 850 °C under pure CO_2 in a PTGA for four coal chars with ranks ranging from subbituminous to anthracite [22]. The pressure dependence is strongest in the lower pressure range, as expected. But the asymptotic saturation at high pressures becomes less pronounced with chars of progressively lower rank. Indeed, no asymptotes are apparent with any of the three subbituminous chars.

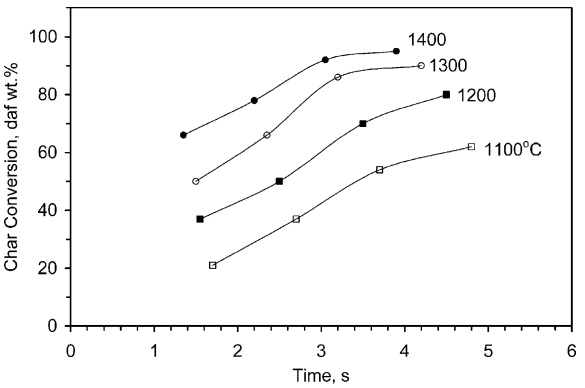

Fig. 8. Char conversion histories of Roto subbituminous char at (●) 1400, (○) 1300, (■) 1200, and (□) 1100 °C and 1.0 MPa under 20% H_2O in a PDTF [25].

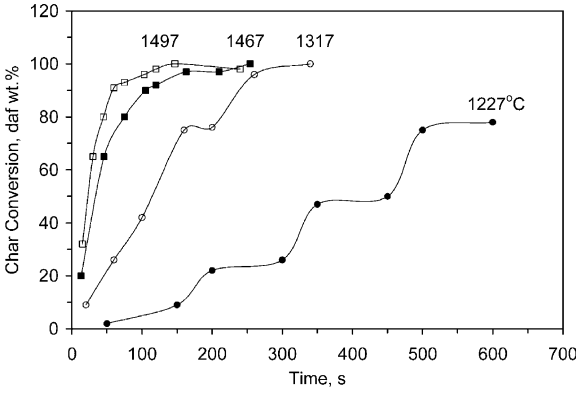

Fig. 9. Char conversion histories of El Cerejon bituminous char at (●) 1227, (○) 1317, (■) 1467, and (□) 1497 °C and 1.5 MPa under 2.5% CO_2 in a WMR [17].

The high rank Hongei char has the slowest gasification rate, by far, across the entire range of pressures. The other three coals, Taiheyo, Yallourn, and Baiduri, are low rank coals, and their gasification rate does not correlate with the carbon content in the parent coal. For example, Yallourn coal contains 69.8 daf wt% carbon, the lowest in this sample suite, but its gasification rate is much slower than Taiheyo char's. Among chars of subbituminous and lower rank, cation mineral contents are more important factors than the overall rank dependence, as explained in the literature [31].

Fig. 11 shows the gasification rates for four bituminous coal chars at 1000 °C under pure CO_2 in a WMR [11]. These measurements were recorded with whole coals, and the char conversion was assigned from the total devolatilization yield obtained in separate tests under inert gases at the same operating conditions. The most remarkable aspects are the diverse responses to the pressure variations among these four samples. The gasification rates of Drayton and El Cerejon are essentially independent of pressure, whereas the Ill. #6 data exhibit the expected enhancements along

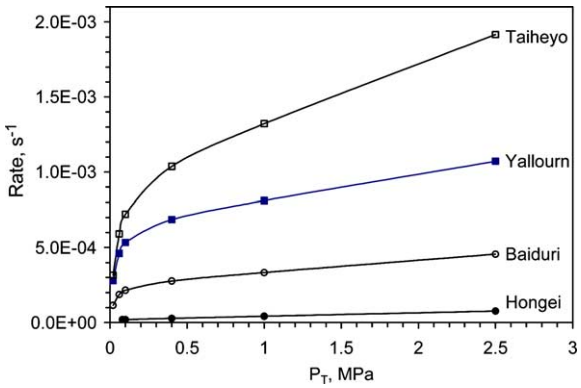

Fig. 10. Gasification rates of (●) Hongei, (○) Baiduri, (■) Yallourn and (□) Taiheyo char at 850 °C in pure CO_2 in a PTGA [22].

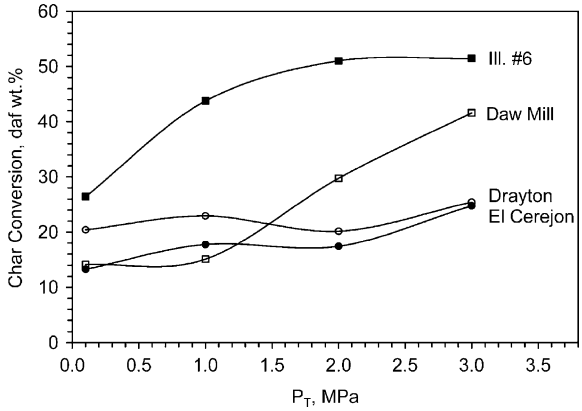

Fig. 11. Gasification rates of (●) El Cerejon, (○) Drayton, (■) Ill. #6 and (□) Daw Mill char at 1000 °C in pure CO_2 for 11 s in a WMR [11].

a saturation curve. The Daw Mill behavior is comparable, except for the insensitivity to pressure variations up to 1.0 MPa. These extents of conversion do correlate well with the carbon contents of the parent coals. Ill. #6 has the lowest carbon content, at 78.2 daf wt%, and is the most reactive across the entire pressure range.

In general, gasification rates diminish for coals of progressively higher rank, but only for ranks of hv bituminous and higher. Mineral catalysis becomes more significant than the generic rank dependence for low-rank chars, so the carbon content of the parent coal no longer correlates this portion of the rank dependence.

3. A reaction mechanism for char gasification

Any plausible reaction mechanism for char gasification must interpret the following trends. With uniform gas composition, gasification rates increase for progressively higher pressures, especially at lower pressures. Whereas the pressure effect saturates at the higher pressures with bituminous chars, no saturation is evident with low-rank chars. With fixed partial pressures of the gasification agents, the pressure effect is much weaker. It may only appear under operating conditions where pore diffusion is the rate controlling mechanism. Gasification rates increase for progressively higher gas temperatures. Our interpretation is based on a new mechanism that incorporates gasification surface kinetics into the framework of Hurt's Carbon Burnout Kinetics (CBK) model. Following an overview of CBK, this section presents the surface gasification mechanism, followed by rate constants, the derivation of an effectiveness factor, the annealing mechanism, ash inhibition, and equilibration of the gas phase composition.

3.1. Overview of CBK/G

CBK is a kinetics package that describes char conversion under conditions relevant to pulverized fuel (p.f.) processes. It was developed by Prof. Robert Hurt both at Sandia National Laboratories, Livermore, and currently, at Brown University. Detailed publications on the earlier versions of CBK [32–35] and the recent extended version for pressurized char oxidation (CBK/E) [2,36] are available. The expanded version for gasification is called CBK/G. It predicts the rate of gasification, the char particle temperature, and the changes in the particle diameter and density as gasification proceeds, given a gas temperature, radiative exchange temperature, and partial pressures of the gasification agents. It is specially designed for carbon conversion applications, because it treats the late stages of char conversion in detail.

Within the theory for char gasification, char reactivity is a dynamic function of heat treatment severity, based on a distributed activation energy model of thermal annealing. The thermal annealing mechanism acts to destroy active sites before the char begins to react. Chars are annealed during heat-up and devolatilization, and throughout gasification. The annealing kinetics are so fast that, practically speaking, the maximum temperature determines the extent of reduction of the intrinsic reactivity due to annealing. The theory uses mass-specific intrinsic kinetics, and earlier versions emphasized the statistical variability of intrinsic char gasification reactivity. There is a standard model of the reaction/diffusion process within porous char particles, and the 'one-film' description of the boundary layer processes to predict gasification rates over a wide range of conditions, including zones I, II, and III and their transitional regimes. The code also includes a model of the effect of ash inhibition on the latest stages of combustion. Together, these mechanisms act to significantly reduce char gasification rates during the later stages of conversion, in accord with observations of very long reaction times for conversion of the last few percentage points of the char mass.

The transport rate of reactant gases to the char surface is determined by bulk diffusion through an external boundary layer, in series with pore diffusion through an ash layer that forms over the char surface during the later stages, in series with pore diffusion through the pore system of the carbonaceous char core. These transport mechanisms must balance the consumption of reactant gases in the chemical reaction mechanism. The model contains an intrinsic formulation that allows a transition to zone 1, in which the gasification agents completely penetrate the internal pore structure and both external film and intraparticle diffusion resistances are negligible. This can be important when overall gasification rates are slow and/or particles are small, which occur naturally at lower temperatures or during the latest stages of char conversion. As an option, the theory contains fuel-general correlations for each of the reactivity parameters, so that predictions can be made knowing only the proximate and ultimate analyses of the parent coal.

CBK has recently been extended and validated for high pressure applications [2,36], with all the same transport-related and annealing mechanisms, including single-film char combustion, intraparticle reaction/diffusion, thermal annealing, and ash inhibition. The new three-step intrinsic kinetics incorporated into CBK/E resolve the problems in the reaction order for conventional char oxidation kinetics. CBK/E also incorporates a correlation of swelling ratio with respect to pressure. CBK/G was developed from the platform of CBK/E. The same annealing submodel and treatments of internal reaction, pore diffusion, and ash inhibition was retained in CBK/G. The additional features required for the extension to gasification are kinetic rate laws for heterogeneous reactions involving CO_2, H_2O, H_2, CO and CH_4, definitions for the associated effectiveness factors and effective diffusivities, a description of pore evolution during char conversion, and an option for equilibration of the gasification agents throughout char conversion.

3.2. Heterogeneous reaction mechanism

A combined oxidation/gasification mechanism was assembled [37] that involves the three reactions for char oxidation in CBK/E plus four reactions for gasification. The mechanism is given in eight steps, of which two are assumed reversible yielding a total of ten heterogeneous reactions, as follows:

Combustion

$$2C + O_2 \rightarrow C(O) + CO \quad (1)$$

$$C + C(O) + O_2 \rightarrow CO_2 + C(O) \quad (2)$$

$$C(O) \rightarrow CO \quad (3)$$

Gasification

$$C + CO_2 \leftrightarrow C(O) + CO \quad (4)$$

$$C(O) \rightarrow CO \quad (5)$$

$$C + H_2O \leftrightarrow C(O) + H_2 \quad (6)$$

$$C(O) \rightarrow CO \quad (7)$$

$$C + 2H_2 \rightarrow CH_4 \quad (8)$$

where C(O) is the oxide complex on the carbon surface. Note that both CO_2 and steam gasification involve oxide complexes with the same nominal composition, but these complexes desorb at different rates. The ratio of the desorption rates, $\gamma = k_7/k_5$, in the rate expressions depends on temperature but not pressure. This variation was invoked after an earlier version of CBK/G with a common oxide complex failed to describe the different

asymptotic limits for steam and CO_2 gasification at the highest pressures.

From the above reaction mechanism, the following rate expressions can be derived by requiring the oxide complex pool to be in pseudo-steady-state:

$$R_{\text{C-Com}} = (k_1 k_2 P_{O_2}^2 + k_1 k_3 P_{O_2})/(k_1 P_{O_2} + k_3/2) \quad (9)$$

$$\text{CO/CO}_2 \text{ from combustion} = k_3/(k_2 P_{O_2}) \quad (10)$$

$$R_{\text{C-Gas}} = (k_7 + k_5)\theta + k_8 P_{H_2} \quad (11)$$

$$R_{\text{C-Total}} = R_{\text{C-Comb}} + R_{\text{C-Gas}} \quad (12)$$

$$R_{O_2} = -(k_1 k_3 P_{O_2}/2 + k_1 k_2 P_{O_2}^2)/(k_1 P_{O_2} + k_3/2) \quad (13)$$

$$R_{H_2O} = -\frac{k_7 k_6 P_{H_2O}}{k_7 + \gamma k_4 P_{CO_2} + \gamma k_4' P_{CO} + k_6 P_{H_2O} + k_6' P_{H_2}} \quad (14)$$

$$R_{CO_2} = -\frac{k_7 k_4 P_{CO_2}}{k_7 + \gamma k_4 P_{CO_2} + \gamma k_4' P_{CO} + k_6 P_{H_2O} + k_6' P_{H_2}} + k_2 k_1 P_{O_2}^2/(k_1 P_{O_2} + k_3/2) \quad (15)$$

$$R_{CO} = k_1 k_3 P_{O_2}/(k_1 P_{O_2} + k_3/2) + 2R_{CO_2} + R_{H_2O} \quad (16)$$

$$R_{H_2} = R_{H_2O} - 2k_8 P_{H_2} \quad (17)$$

$$R_{CH_4} = k_8 P_{H_2} \quad (18)$$

where

$$\theta = \frac{k_4 P_{CO_2} + k_6 P_{H_2O}}{k_7 + \gamma k_4 P_{CO_2} + \gamma k_4' P_{CO} + k_6 P_{H_2O} + k_6' P_{H_2}} \quad (19)$$

and the rate constants k_i, $i = 1, 8$, have the Arrhenius form.

The above mechanism and the rate expressions are based on several assumptions. First, the mechanism assumes different but coexisting surface oxides, C(O), for CO_2 and H_2O gasification. The desorption rates of these C(O) are different, so that the CO_2 and steam gasification rates saturate to different limits at very high pressures.

Second, the mechanism does not include CO chemisorption nor the accompanying reactions of C(CO), which give rise to quadratic higher order terms in the Langmuir–Hinshelwood rate expressions in some other mechanisms [30,38,39]. For example, in Mühlen's work, the rate expression for mixtures of CO_2, H_2O, CO, H_2 is

$$R_{\text{C–Gas}} = \frac{k_1 P_{CO_2} + k_8 P_{CO_2}^2 + k_9 P_{H_2O} + k_{11} P_{H_2O}^2 + k_{12} P_{H_2O} P_{H_2} + k_4 P_{H_2}}{1 + k_2 P_{CO_2} + k_3 P_{CO} + k_{10} P_{H_2O} + k_5 P_{H_2}} \quad (20)$$

Note that this rate expression is given as specified in Mühlen et al. [30], and the indices on the rate constants do not pertain to the same reactions in our mechanism.

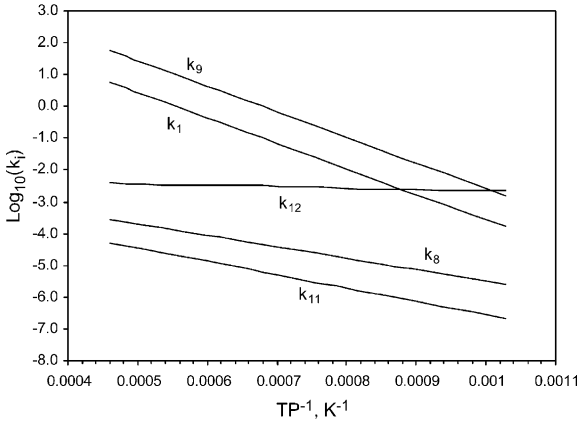

Fig. 12. Comparison of rate constants in quadratic and first-order terms in Eq. (20) assigned by Mühlen et al. [30].

The Arrhenius diagram for Mühlen's rate law in Fig. 12 shows that the rate constants k_8, k_{11} and k_{12} in the quadratic terms in Eq. (20) are small compared to k_1 and k_9 in the first-order terms at temperatures above 900 °C. In an entrained flow gasifier where the typical gas temperature is between 1500 and 2000 °C, the rate constants of the quadratic terms are 3–5 orders of magnitude smaller than those for the first-order terms. In a fluidized bed gasifier where temperatures are below 900 °C, only k_{12} is comparable to the constants for the first-order terms. For mathematical simplicity, we ignored all quadratic terms in deriving the rate expressions in Eqs. (14)–(19).

Third, combustion and gasification do not share a common oxide complex pool for two reasons. First, if the oxide pools for gasification and combustion were assumed identical, the desorption-limited rates for both processes would be identical, a constraint that would make it difficult to predict some of the observed CO_2/H_2O kinetic data. Second, oxidation is much faster than gasification at low temperatures where oxide coverage is significant, so a significant competition for the oxide sites never arises in practice and is not necessary to include in the model. For mathematical simplicity, our mechanism assumes that the active sites for oxidation are independent of those for gasification. Based on similar reasoning, H_2 gasification is also independent of gasification by CO_2 and steam because its rate is several orders of magnitude slower. The kinetics for hydrogasification are resolved separately.

3.3. Rate constants

In the rate expressions in Eqs. (9)–(19), 10 rate constants need to be specified. These rate constants include k_i ($i = 1$–4 and 6–8), two reverse reaction rate constants k_4' and k_6', and the ratio of k_7 to k_5. The constants k_1, k_2, k_3 involved in the rate expression for char oxidation have been discussed in detail by Hurt and

Calo [36], and are not presented here. The other rate parameters are specified in this section. Additional details were reported separately [40].

Fig. 13 shows Arrhenius plots of k_5, k_4 and k_4' obtained from five datasets on high-pressure CO_2 gasification [19,22,23,30,39]. The char types ranged from lignite to anthracite.

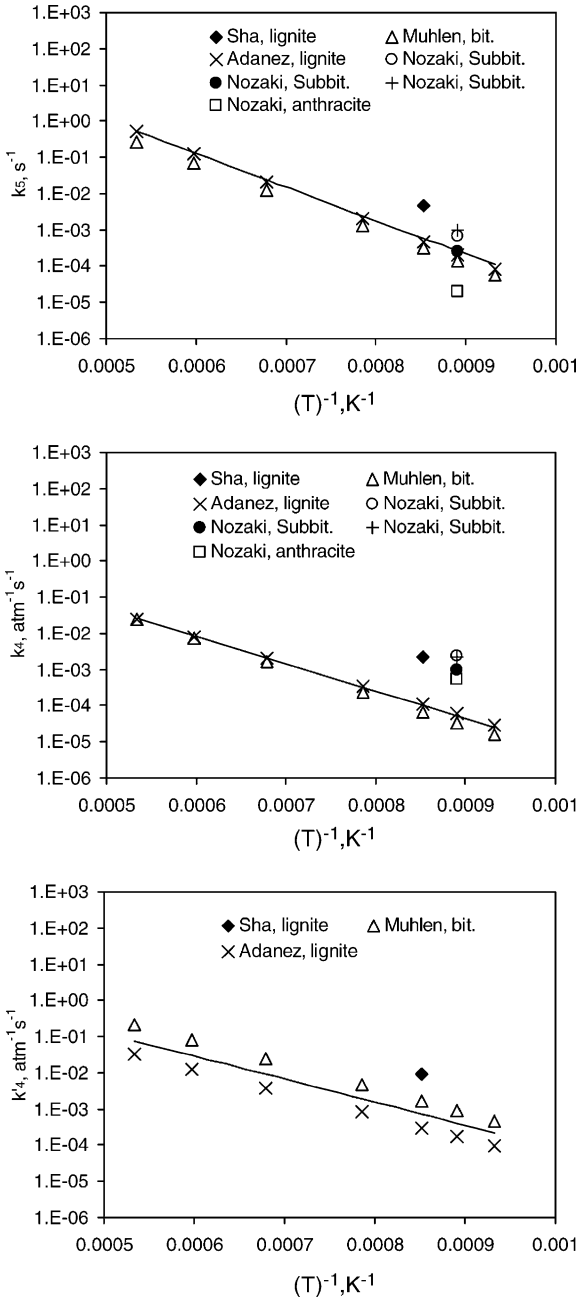

Fig. 13. Arrhenius plots of (upper) k_5, (middle) k_4 and (lower) k_4' specified from CO_2 gasification datasets. Solid lines represent mean values incorporated into CBK/G.

The rate constants based on datasets by Adánez et al. [23] and Mühlen et al. [30] were extrapolated using the rate expressions assigned from the data, whereas those from Sha et al. [19] and Nozaki et al. [22] appear only at the test temperatures. At 850 °C, k_5 for the desorption of the surface complex varies over two orders of magnitude, and generally increases as coal rank decreases. Lignite char has the highest k_5-value among all types. The activation energy for desorption from datasets by Mühlen et al. [30] and Adánez et al. [23] is 180 kJ/mol.

The adsorption rate constant k_4 also varies over two orders of magnitude. The E_4-vales from Mühlen et al. [30] and Adánez et al. [23] are 153 and 140 kJ/mol, respectively. The rate constant k_4' is probably comparable to k_4, which expresses significant inhibition by CO. Values for E_4' from Mühlen et al. and Adenaz et al. were 128 and 122 kJ/mol, respectively.

The values for k_5, k_4 and k_4' used in CBK/G appear as solid lines in Fig. 13, based on the pre-exponential factors and the activation energies in Table 4.

Fig. 14 shows Arrhenius plots for k_7, k_6 and k_6' from four datasets on high pressure steam gasification [19–21,30], which cover char types from lignite through anthracite. At 850 °C, k_7 varies over one and a half orders of magnitude, with lignite char having the highest value. Values for E_7 vary from 80 to 170 kJ/mol, where Goyal et al. [21] reported the lowest value. The activation energies for k_6 are 150–160 kJ/mol in Ma et al. [20] and Mühlen et al. [30], and 210 kJ/mol in Goyal et al. [21]. For the reverse adsorption reaction k_6', activation energies of 62 and −185 kJ/mol were reported by Goyal et al. and Mühlen et al., respectively. The negative value of E_6' from Mühlen et al. is poorly understood. We adopted k_6' from Goyal et al. for CBK/G. The mean pre-exponential factors and activation energies in k_7, k_6 and k_6' appear in Table 4.

For the domain of operating conditions in advanced technologies, the overall gasification rate is controlled by both adsorption and desorption. It is worth noting that the activation energies for desorption, E_5 and E_7, are slightly higher than those for adsorption, E_4 and E_6, suggesting that the reaction order with respect to the partial pressures of reactants will only slightly increase with temperature. Little data are available to verify this expectation, because most of

Table 4
Mean pre-exponential factors and activation energies for the rate constants in Eqs. (10)–(19)

Rate constant	A_0-value	E (kJ/mol)
k_4	293 $atm^{-1}\,s^{-1}$	145
k_4'	192 $atm^{-1}\,s^{-1}$	122
k_6	4.0×10^3 $atm^{-1}\,s^{-1}$	160
k_6'	3 $atm^{-1}\,s^{-1}$	70
k_7	4.1×10^4 s^{-1}	176
k_8	3.24 $atm^{-1}\,s^{-1}$	150

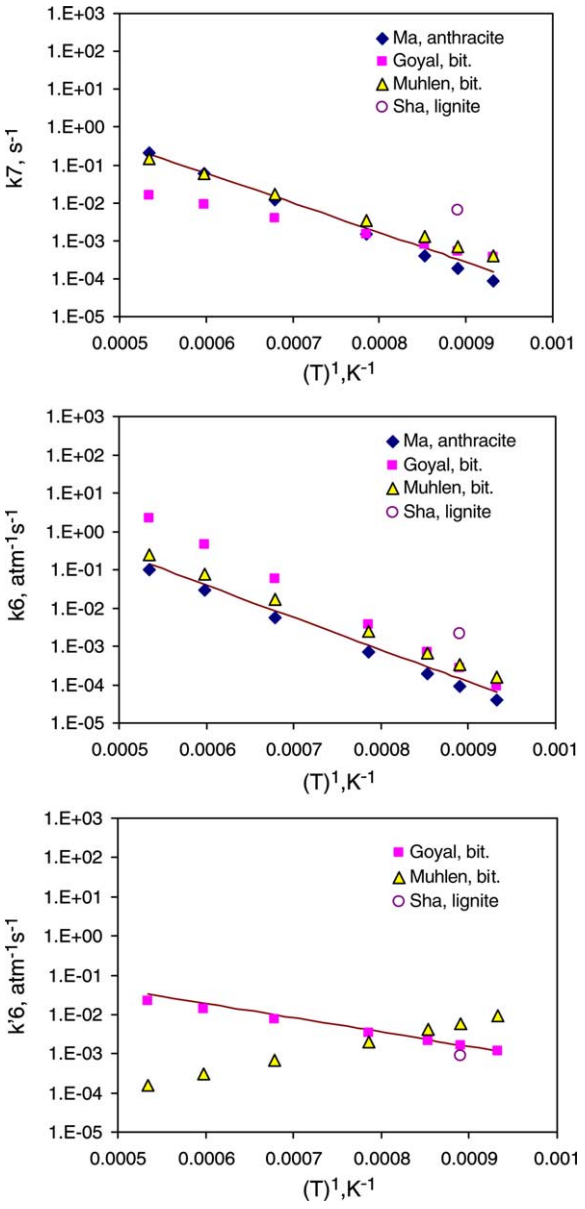

Fig. 14. Arrhenius plots of (upper) k_7, (middle) k_6 and (lower) k_6' specified from H_2O gasification datasets. Solid lines represent mean values incorporated into CBK/G.

the reported gasification kinetics were measured below 1000 °C. A recent study by Kajitani et al. [24] showed that the reaction order for CO_2 gasification increased from 0.54 to 0.73 as temperatures were increased above 1200 °C. Although it is difficult to assign accurate kinetic parameters from data in zone II, we can reasonably expect reaction orders greater than 0.5.

Three datasets reported both CO_2 and steam gasification rates for the same fuel, from which γ, the ratio of desorption rates of steam and CO_2 gasification, can be estimated. The assigned value was about 4 for the lignite in Sha et al.'s dataset, and about 10 for a bituminous coal in Kajitani et al. Roberts and Harris [26] reported a value of about 12 for both a bituminous and an anthracite.

The H_2 gasification rate is several orders of magnitude slower than those for CO_2 or steam [41]. Hydrogasification is not as well understood and only a few investigations are available [27,42,43]. Among these investigations, Blackwood [42] and Tomita et al. [43] used a first-order rate expression. The activation energy reported by Tomita et al. ranged from 59 to 217 kJ/mol versus Blackwood's value of 125 kJ/mol. Li and Sun [27] used a half-order rate expression with an activation energy of 196.6 kJ/mol. As presented in Section 4.1, we use the first-order H_2 gasification rate with an activation energy of 150 kJ/mol.

3.4. Effectiveness factor

The effectiveness factor η needs to be evaluated for two reasons. First, its magnitude identifies the gasification regime, which for gasification in practical applications is either chemical reaction control (zone I) or mediation by internal pore diffusion (zone II). Second, it also accounts for internal pore diffusion effects in the calculation of the overall rate of carbon gasification in zone II. Char oxidation and CO_2 and H_2O gasification are assigned separate effectiveness factors. The former has already been implemented in CBK/E [2] and is not discussed here. The hydrogasification of char occurs in zone I under even entrained gasification conditions, so the effectiveness factor for hydrogasification can be assumed to be unity.

From the kinetic rate laws in Section 3.2, the CO_2 and steam gasification rates $R_{C\text{-}CO_2}$ and $R_{C\text{-}H_2O}$ are expressed without the quadratic terms as follows:

$$R_{C\text{-}CO_2} = \frac{k_7 k_4 P_{CO_2}}{k_7 + \gamma k_4 P_{CO_2} + \gamma k_4' P_{CO} + k_6 P_{H_2O} + k_6' P_{H_2}} \tag{21a}$$

$$R_{C\text{-}H_2O} = \frac{k_7 k_6 P_{H_2O}}{k_7 + \gamma k_4 P_{CO_2} + \gamma k_4' P_{CO} + k_6 P_{H_2O} + k_6' P_{H_2}} \tag{21b}$$

which simplifies to:

$$R_{C\text{-}CO_2} = \frac{K_{1a} P_{CO_2}}{1 + K_2 P_{CO_2} + K_3 P_{H_2O}} \tag{22a}$$

$$R_{C\text{-}H_2O} = \frac{K_{1b} P_{H_2O}}{1 + K_2 P_{CO_2} + K_3 P_{H_2O}} \tag{22b}$$

where $K_{1a} = k_7 k_4/\omega$; $K_{1b} = k_7 k_6/\omega$; $K_2 = (\gamma k_4 - 2\gamma k_4' D_{CO_2}/D_{CO})/\omega$; $K_3 = (k_6 - k_6' D_{H_2O}/D_{H_2} - \gamma k_4' D_{H_2O}/D_{CO})/\omega$; and $\omega = k_7 + \gamma k_4'(P_{CO,S} + 2P_{CO_2,S} D_{CO_2}/D_{CO} + P_{H_2O,S} D_{H_2O}/D_{CO}) + k_6'(P_{H_2,S} + P_{H_2O,S} D_{H_2O}/D_{H_2})$

Following Hong's [44] derivation of the effectiveness factor for Langmuir–Hinshelwood type rate expressions, we

first determine the effective reaction orders for R_{CO_2} and R_{H_2O} as follows:

$$n_{CO_2} = 1 - \frac{K_2 \bar{P}_{CO_2}}{1 + K_2 \bar{P}_{CO_2} + K_3 \bar{P}_{H_2O}} \tag{23a}$$

$$n_{H_2O} = 1 - \frac{K_3 \bar{P}_{H_2O}}{1 + K_2 \bar{P}_{CO_2} + K_3 \bar{P}_{H_2O}} \tag{23b}$$

where $\bar{P}_{CO_2} \approx P_{CO_2,S}$ and $\bar{P}_{H_2O} \approx P_{H_2O,S}$ are the mean partial pressures of CO_2 and H_2O within the porous char particle.

The Thiele moduli are defined as

$$\phi_{CO_2} = \frac{d_P}{2}\left(\rho \nu_{C\text{-}CO_2} \frac{n_{CO_2}+1}{2D_{CO_2}} \frac{R_{CO_2,S}}{C_{CO_2,S}}\right)^{0.5} \tag{24a}$$

$$\phi_{H_2O} = \frac{d_P}{2}\left(\rho \nu_{C\text{-}H_2O} \frac{n_{H_2O}+1}{2D_{H_2O}} \frac{R_{H_2O,S}}{C_{H_2O,S}}\right)^{0.5} \tag{24b}$$

where ρ is the apparent density of the char, ν is a stoichiometric coefficient whose subscript denotes the gasification reaction; $R_{CO_2,S}$ and $C_{CO_2,S}$ are the reaction rate and the molar concentration of CO_2 at the particle surface, respectively; $R_{H_2O,S}$ and $C_{H_2O,S}$ are the reaction rate and the molar concentration of H_2O at the particle surface, and n_{CO_2} and n_{H_2O} are effective reaction orders. The complex definition for the effective reaction orders arises from the complex rate expressions for the surface kinetics. The effective diffusivities in Eqs. (24a) and (24b) are evaluated as products of the continuum diffusion coefficients and the ratio of total porosity to tortuosity. The tortuosity is re-scaled by the percentage of pore-volume in macropores. Knudsen diffusion through micropores is omitted.

The effectiveness factor is defined as the ratio of the actual rate to the rate if the concentrations of the gasification agents were uniform throughout the char particle, as occurs under chemical reaction control. Following Satterfield [45] we then derive the effectiveness factors for $R_{C\text{-}CO_2}$ and $R_{C\text{-}H_2O}$ as follows:

$$\eta_{CO_2} = \frac{1}{\phi_{CO_2}}\left[\frac{1}{\tanh(\phi_{CO_2})} - \frac{1}{\phi_{CO_2}}\right] \tag{25a}$$

$$\eta_{H_2O} = \frac{1}{\phi_{H_2O}}\left[\frac{1}{\tanh(\phi_{H_2O})} - \frac{1}{\phi_{H_2O}}\right] \tag{25b}$$

The overall rates of char-CO_2 and steam gasification in zone II are given as

$$R_{C\text{-}CO_2} = \eta_{CO_2} \frac{k_7 k_4 P_{CO_2,S}}{k_7 + \gamma k_4 P_{CO_2,S} + \gamma k_4' P_{CO,S} + k_6 P_{H_2O,S} + k_6' P_{H_2,S}} \tag{26a}$$

$$R_{C\text{-}H_2O} = \eta_{H_2O} \frac{k_7 k_6 P_{H_2O,S}}{k_7 + \gamma k_4 P_{CO_2,S} + \gamma k_4' P_{CO,S} + k_6 P_{H_2O,S} + k_6' P_{H_2,S}} \tag{26b}$$

Both η_{CO_2} and η_{H_2O} will vary from 0.2 to 1.0 under typical entrained flow gasification conditions.

The total rate of char gasification by CO_2, H_2O and H_2 is then as follows:

$$R_{C\text{-}Gas} = R_{C\text{-}CO_2} + R_{C\text{-}H_2O} + R_{C\text{-}H_2} \tag{27a}$$

where $R_{C\text{-}H_2} = k_8 P_{H_2}$ is the rate for hydrogasification. The formation and depletion rates for the major gaseous products, CO_2, H_2O, CO and H_2, are then given as:

$$R_{CO_2} = -R_{C\text{-}CO_2} \tag{27b}$$

$$R_{H_2O} = -R_{C\text{-}H_2O} \tag{27c}$$

$$R_{CO} = R_{C\text{-}CO_2} + R_{C\text{-}H_2O} \tag{27d}$$

$$R_{H_2} = R_{C\text{-}H_2O} - 2R_{C\text{-}H_2} \tag{27e}$$

3.5. Gas transport in the boundary layer

The partial pressures of reactant gases in the ambient atmosphere surrounding the particle must be specified to evaluate gasification rates. However, the overall rates are actually calculated from the partial pressures at the particle surface $P_{CO_2,S}$, $P_{H_2O,S}$, $P_{CO,S}$ and $P_{H_2,S}$ in Eqs. (27b)–(27e). The surface partial pressures are related to the ambient composition by the following four coupled non-linear transport equations for gases in the boundary layer around the particle:

$$P_{CO_2,S} = P_{CO_2,\infty} - \frac{q_{CO_2}}{k_{D,CO_2}} \tag{28}$$

$$P_{H_2O,S} = P_{H_2O,\infty} - \frac{q_{H_2O}}{k_{D,H_2O}} \tag{29}$$

$$P_{CO,S} = P_{CO,\infty} - \frac{q_{CO}}{k_{D,CO}} \tag{30}$$

$$P_{H_2,S} = P_{H_2,\infty} - \frac{q_{H_2}}{k_{D,H_2}} \tag{31}$$

where $P_{i,\infty}$ is the partial pressure of gas i in the ambient atmosphere; $k_{D,i}$ is the mass transfer coefficient for gas i; and q_i is the *depletion* flux of gas i due to reaction, which can be evaluated from the gasification rates, R_i, using Eq. (32):

$$q_i = \frac{d_P}{6}\rho R_i \tag{32}$$

and R_i can be evaluated through Eqs. (27b)–(27e). Eqs. (28)–(31) are coupled non-linear equations for $P_{CO_2,S}$, $P_{H_2O,S}$, $P_{CO,S}$ and $P_{H_2,S}$, which we solve with a least-squares Levenberg–Marquant algorithm.

3.6. Annealing mechanism

Annealing is important in entrained flow gasification where char particles experience very high temperatures. Annealing mechanisms and kinetics for char gasification at annealing temperatures as high as 2000 °C have been characterized [46]. The magnitude of this effect likely varies for each gasification agent, due to differences among catalyst activity and active site pools. However, the current literature cannot define separate annealing laws for the ten heterogeneous reactions in our mechanism. The assumption of equal deactivation factors for all the heterogeneous reactions is necessary at this time.

The dynamic annealing model in CBK was incorporated into CBK/G assuming equal deactivation factors for all heterogeneous reactions:

$$A_i/A_{i0} = f(T_{HT}, t_{HT}) \tag{33}$$

where A_i represents all the pre-exponential factors in the kinetic mechanism; T_{HT} and t_{HT} represent the temperature and duration of heat treatment, respectively.

For gasification by CO_2 and steam, the global gasification rate expression can be rearranged as follows:

$$R_{C\text{-}Gas} = k_7 \frac{\frac{k_4}{k_7}P_{CO_2} + \frac{k_6}{k_7}P_{H_2O}}{1 + \gamma\frac{k_4}{k_7}P_{CO_2} + \gamma\frac{k_4'}{k_7}P_{CO} + \frac{k_6}{k_7}P_{H_2O} + \frac{k_6'}{k_7}P_{H_2}} \tag{34}$$

The annealing mechanism is implemented by adjusting only the pre-exponential factor in k_7, according to Eq. (33), and by maintaining constant ratios for k_4/k_7, k_4'/k_7, k_6/k_7 and k_6'/k_7. The same procedure has already worked well in CBK/E.

3.7. Physical transformations

Gasification chemistry transforms a char's physical structure throughout conversion. In CBK/E, the empirical correlations for particle diameter and density to describe these transformations are:

$$\frac{\rho}{\rho_0} = \left(\frac{m}{m_0}\right)^{\alpha} \tag{35}$$

$$\frac{d_P}{d_{P0}} = \left(\frac{\rho}{\rho_0}\right)^{-1/3}\left(\frac{m}{m_0}\right)^{1/3} \tag{36}$$

where ρ denotes the particle density, d_P denotes the particle diameter; and m denotes the particle mass. Subscript 0 denotes the initial value. Values of α for gasification are specified from the following correlation [47]:

$$\alpha = \frac{\beta}{3+\beta} \tag{37}$$

where $\beta = d_P S\eta/2$, S is the internal surface area per volume, and η is the effectiveness factor. For a 60-μm char particle with 10 m^2/g surface area and 600 kg/m^3 apparent char density, the effectiveness factor is between 0.2 and 1.0 in entrained flow gasification. The value of α is then estimated to be between 0.95 and 1. In fluidized beds, reaction temperatures are low, but the particle size is larger. A value of 0.95 is used for both entrained and fluidized bed gasification.

Two independent mechanisms are responsible for surface area evolution during gasification. One is caused by reaction alone, which can be represented by the random pore model [48–50]. The other one is due to annealing. For gasification at low temperatures in fluidized beds for example, surface area evolution due to reaction is significant, and a random pore model quantitatively describes the evolution. In entrained flow gasification, however, annealing plays the more important role. Under these conditions, char reactivities often correlate poorly with total surface area [51,52]. Surface areas measured in a number of separate entrained flow reactor experiments where chars are generated in situ show monotonic decreases in area during reaction when the areas are normalized by the mass of char remaining (see for example Hurt et al. [33]). The traditional geometrical and random pore models predict the opposite trend. CBK/G contains an annealing submodel as well as the random pore model to describe both mechanisms for area evolution.

The random pore model is implemented by imposing the following factor into the gasification rate to account for the loss of surface area due to carbon conversion:

$$f_{RPM} = \sqrt{1 - \psi_0 \ln(1-X)} \tag{38}$$

where X is the fraction of carbon converted; and ψ_0 is a structural parameter that can be estimated by fitting gasification data. Zolin [53] reported ψ_0 values ranging from 2.2 to 19 for nine coal chars of different rank from their gasification measurements. The ψ_0 values of eight of these chars are in a range of 2.2–7.7. We applied a mean ψ_0 of 4.6 in CBK/G for all char types.

3.8. Ash inhibition

CBK/E contains a mechanism for ash film formation and its effect on mass and heat transfer into the particle. Under almost all conditions in conventional p.f. combustion, such ash inhibition is negligible. Recent data from CRIEPI, however, on coals with 33–53 wt% ash [54] suggest that such effects may be important in unusual cases. They may also be important in biomass char gasification, due to the very high char ash levels associated with the very high volatile yields. For this reason, and because the ash inhibition submodel in CBK/E does not add significantly to the computational burden, it was carried over into CBK/G.

3.9. Gas phase equilibration

For gasification at the highest temperatures with realistic suspension loadings, the local gas composition may be equilibrated. This situation is described with an expanded version of Penner's [55] equilibrium calculation for hydrocarbon systems, involving 18 species (CO, CO_2, NO, H, O, OH, O_2, H_2, H_2O, CH_4, C(g), C(s), C_2H_2, HCN, NH_3, NO_2, N, N_2) and four elemental balances.

4. Model evaluations

4.1. Simulation procedures

CBK/G was incorporated into NEA's PC Coal Lab®, a comprehensive computer package for the combustion of individual particles of any coal, biomass, or petroleum coke at any operating conditions. PC Coal Lab® already incorporates NEA's FLASHCHAIN® for devolatilization, simplified mechanisms for secondary volatiles pyrolysis and volatiles combustion, and CBK/E for char oxidation. Once CBK/G was built into PC Coal Lab®, the package was used to simulate coal and char conversion for the operating conditions in each individual test in the database. The only required fuel-specific data were the proximate and ultimate analyses of the parent coal. Operating conditions were specified as the reactor type—either PDTF or WMR, pressure, initial particle temperature, gas temperature, wall temperature, the mole fractions of CO_2, H_2O, CO and H_2, reaction time and particle size. Some cases were better described with profiles of gas temperature, wall temperature, and reactant mole fractions. All these assignments were taken directly from the reported test conditions for each dataset.

In tests with whole coals, FLASHCHAIN® predicted the residual char yield and char properties that were subject to gasification during later stages of the test. In tests with chars, FLASHCHAIN® was used in separate simulations of the char preparation conditions to determine the char properties which, in turn, were used as the input for the gasification test simulations. Diminished gasification reactivity due to annealing during char preparation was accounted for in CBK/G by evaluating the annealing rate over the temperature history during the preparation stage prior to the gasification simulation.

Thirteen rate parameters listed in Table 5 appear in CBK/G. As described in Section 3.6, the rate constants for adsorption and reverse adsorption are expressed as constant ratios k_4/k_7, k_4'/k_7, k_6/k_7 and k_6'/k_7, to expedite the implementation of annealing. This form also facilitates implementation of rank effects, which are imposed on all steps in the reaction mechanism by adjusting only A_{70}. All rate parameters in Table 5 except A_{70} were set to their default values in the data evaluations. The default values were either constants or determined by correlations, as indicated in Table 5. The correlations were established from the kinetics studies in Section 3.3 with fine tuning during pre-evaluations against the entire database. The rank dependent correlations for A_{40}/A_{70}, A'_{40}/A_{70}, A_{60}/A_{70}, A'_{60}/A_{70}, γ and E_7 are as follows:

Table 5
Rate parameters involved in CBK/G and their default values

Rate parameter	Value
A_{70} (s^{-1})	Adjusted
A_{40}/A_{70} (atm^{-1})	Correlation Eq. (39)
A'_{40}/A_{70} (atm^{-1})	Correlation Eq. (40)
A_{60}/A_{70} (atm^{-1})	Correlation Eqs. (41a) and (41b)
A'_{60}/A_{70} (atm^{-1})	Correlation Eq. (42)
A_{80}/A_{70} (atm^{-1})	7.9×10^{-5}
$\gamma=A_{70}/A_{50}$ (–)	Correlation Eq. (43)
E_7 (kJ/mol)	Correlation Eq. (44)
E_4-E_7 (kJ/mol)	54
E'_4-E_7 (kJ/mol)	−53.9
E_6-E_7 (kJ/mol)	−16
E'_6-E_7 (kJ/mol)	−156
E_8-E_7 (kJ/mol)	−26

$$A_{40}/A_{70} = 1.84\times10^{3}\exp(-0.073C_{daf}) \quad (39)$$

$$A'_{40}/A_{70} = 3.57\times10^{-5}C_{daf} - 1.73\times10^{-3} \quad (40)$$

$$A_{60}/A_{70} = 0.05 \ \ (C_{daf}\le 90.6) \quad (41a)$$

$$A_{60}/A_{70} = 0.021C_{daf} - 1.86 \ \ (C_{daf} > 90.6) \quad (41b)$$

$$A'_{60}/A_{70} = -3.68\times10^{-8}C_{daf} + 3.2\times10^{-6} \quad (42)$$

$$\gamma = 6.92\times10^{2}\exp(-5.0\times10^{4}/RT) \quad (1073\le T,\ K\le 1573) \quad (43)$$

$$E_7 = 3.52C_{daf} - 131.1 \quad (44)$$

where C_{daf} is the daf carbon content of coal. All parameters except γ are rank dependent. In Eq. (43), if temperature is beyond the range, 800 and 1300 °C should be used for lower and higher temperatures, respectively. The correlations in Eqs. (39)–(44) implicitly reflect a host of kinetic submechanisms in CBK/G, as well as supplemental variations with coal quality, including estimates for the coal density and the density of combustibles in char. These correlations should not be incorporated into other char gasification mechanisms unless all the supplemental information is also the same. They also need to be modified whenever the supplemental information is upgraded.

In the fitting of test data, the default value for A_{70} was first assigned to determine a baseline CBK/G prediction for each test case. Its value was adjusted in iterations until the error between the predicted and reported gasification

behavior was less than 5%. Then the assigned values for all test cases in the subject dataset were averaged to assign the best-fit value of A_{70} for that particular fuel. The best-fit values for all fuels in the database were then used to develop a rank-dependent correlation to estimate A_{70} for generalized applications, which is presented in Section 5.2.

The criterion for evaluating the model predictions is the standard error of estimation (SEE), which is defined as follows:

$$\mathrm{SEE} = \sqrt{\frac{\sum_{i=1}^{n_E}(p_i^p - p_i^o)^2}{n_S - n_F - 1}} \tag{45}$$

where p_i^p is the prediction for the ith record; p_i^o is the measured value; n_S is the number of records under evaluation; and n_F is the number of independent factors accounted for in the model. Logarithms of the rates were used in evaluating SEE for gasification rates. The number of independent modeling factors is easiest to specify when the model is a multivariate regression; however, it is ambiguous with mechanistic models like CBK/G. Throughout all the evaluations in this report, n_F was specified as 5 to account for the variations in pressure, gas mole fractions, gas temperature, reaction time, and coal quality. Since n_S is so much greater than unity, the specification on n_F is unimportant.

4.2. Data evaluations

This section presents the evaluations of CBK/G predictions for the entire database. A parity plot for the 228 extents of conversion recorded in individual tests appears in Fig. 15. The predictions are based on the best-fit value for A_{70} for each coal. The reported extents of char conversion uniformly cover the entire range from 0 to 100 daf wt%. Both low and high conversion levels show substantial scatter, although there are no systematic discrepancies in the predictions. The SEE for the predicted conversion is 11.4 daf wt%, so the predictions remain within useful quantitative tolerances.

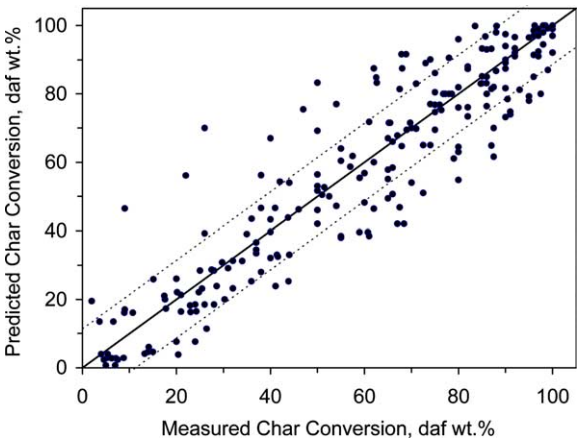

Fig. 15. Parity plot for extent of char conversion based on the best-fit k_7-parameter assignment for each coal. Dotted lines represent prediction uncertainties with the SEE of 11.4 daf wt%.

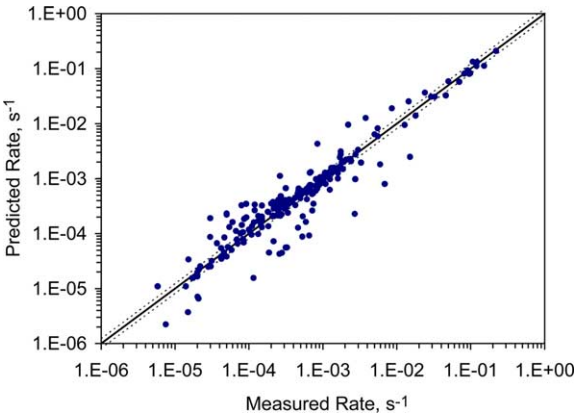

Fig. 16. Parity plot for gasification rate based on the best-fit k_7-parameter assignment for each coal. Dotted lines represent prediction uncertainties with the SEE of 0.1 order of magnitude.

The parity plot of 225 gasification rate predictions appears in Fig. 16. Due to the wide range of operating conditions covered in the database, the gasification rates varied over four orders of magnitude, although most of the reported rates were concentrated within two orders of magnitude. There are no systematic discrepancies in the predictions over this entire range. The SEE for the predicted rates is 0.1 orders of magnitude, which corresponds to a $\pm 22.7\%$ uncertainty. The individual case studies are presented in succeeding sections.

4.2.1. IC datasets

Six datasets from Imperial College were recorded with a pressurized WMR reactor to measure the extents of

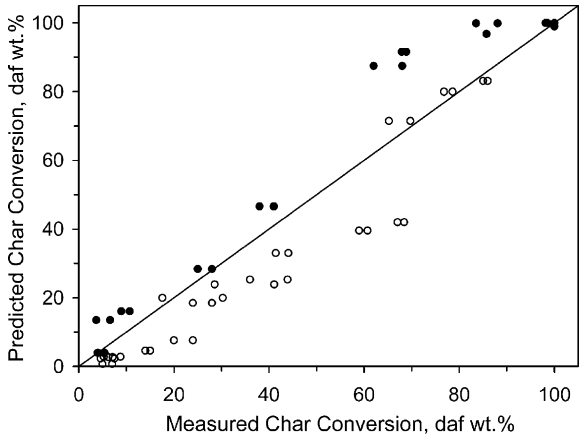

Fig. 17. Parity plot for char conversion for Daw Mill gasification under (●) 80% H_2O and (○) pure CO_2 at 1000 °C, 0.1, 1.0, 2.0 and 3.0 MPa, and holding times of 1, 11, 21 and 61 s in a WMR [9,10].

conversion during steam and CO_2 gasification. These tests heated small amounts of 128 μm coal samples at 1000 °C/s to 1000 °C, then maintained temperature for reaction times of 1, 11, 21 and 61 s. The steam gasification experiments used 80% steam in He at 0.1, 1.0 and 2.0 MPa, whereas CO_2 gasification was monitored under pure CO_2 at 0.1, 1.0, 2.0 and 3.0 MPa. Whole coals were used in the tests, and the char conversion levels were assigned with the char yields monitored in separate pyrolysis tests at the same operating conditions, except for the inert gas environment.

Two separate datasets reported by Messenböck et al. [9,10] characterized the same coal under the same conditions. The parity plot for char conversion in Fig. 17 shows that the char conversion levels were underpredicted for CO_2 gasification, but overpredicted for steam gasification. The CO_2 gasification rate for Daw Mill was also measured by Lim et al. [12]. The parity plot for gasification rate in Fig. 18 shows reasonable agreement. The extents of conversion for Daw Mill gasification in either H_2O or CO_2 were also reported for a reaction time of 61 s [13,14]. The parity plots for char conversion in Fig. 19 show reasonable agreement.

Messenböck et al. [11] also reported conversion levels for CO_2 gasification for three additional coals at 0.1, 1.0, 2.0 and 3.0 MPa in a WMR at a reaction time of 11 s. These coals are El Cerejon, Drayton, Ill. #6, with carbon contents of 82.4, 82.6, and 78.2 daf wt%, respectively. The parity plot for char conversion in Fig. 20 shows good accuracy for the available cases at high extents of conversion. But the lowest conversion levels for each of the four coals (not shown) were badly underpredicted. This flaw pertains to the tests with all four coals at atmospheric pressure, and may reflect a problem in the apparent reaction order from CBK/G. If the gasification rate was first-order in the CO_2 partial pressure, then the extents of conversion should increase in proportion to the pressure increases. But the reported levels at 0.1 MPa show much higher conversion levels than expected.

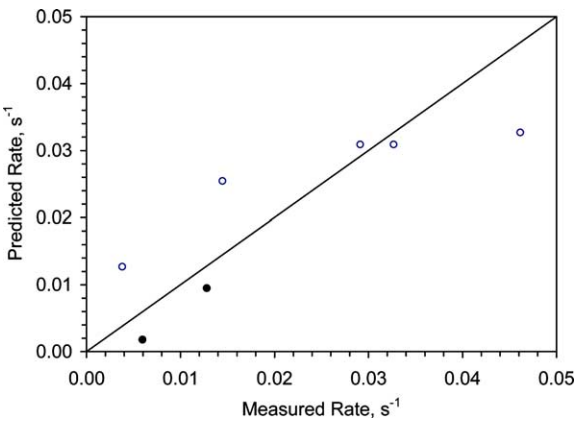

Fig. 18. Parity plot of gasification rate for Daw Mill under pure CO_2 at (●) 850 °C and (○) 1000 °C, 0.1, 1.0, 2.0 and 3.0 MPa, and a reaction time of 11 s in a WMR [12].

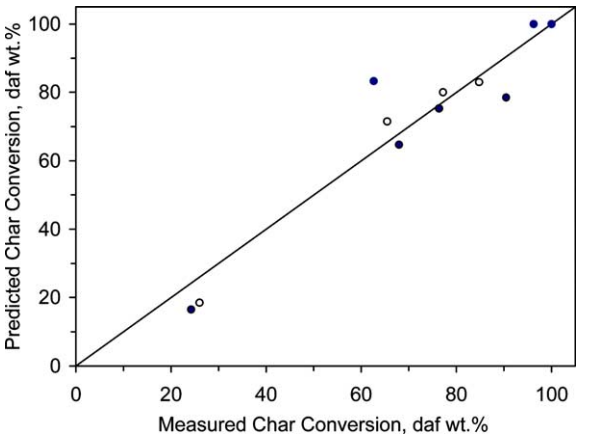

Fig. 19. Parity plot for char conversion for Daw Mill gasification under (●) 80% H_2O and (○) pure CO_2 at 1000 °C, 0.1, 1.0, 2.0 and 3.0 MPa, and reaction times of 61 s in a WMR [13,14].

4.2.2. UAM dataset

The gasification experiments on a hv bituminous char (82.4% C, daf) at the University of Amsterdam [15] were carried out in a PTGA on char that was pyrolyzed in entrained flow at 1100 °C for 1.4 s. Gasification experiments were performed either with H_2O at a partial pressure of 1.2 MPa or with a mixture of H_2O and H_2 at partial pressures of 0.15 and 0.045 MPa, respectively. Temperatures were varied from 813 to 925 °C.

The gasification rates for a range of char conversion are evaluated in Fig. 21. Under all operating conditions, both the predicted and observed gasification rates decrease for progressively higher extents of char conversion. For steam

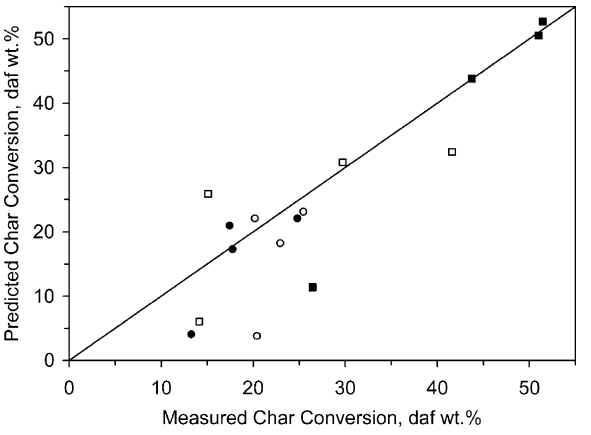

Fig. 20. Parity plot for char conversion for gasification of (●) El Cerejon, (○) Drayton, (■) Ill. #6 and (□) Daw Mill under pure CO_2 after 11 s at 1000 °C and 0.1, 1.0, 2.0 and 3.0 MPa in a WMR [11].

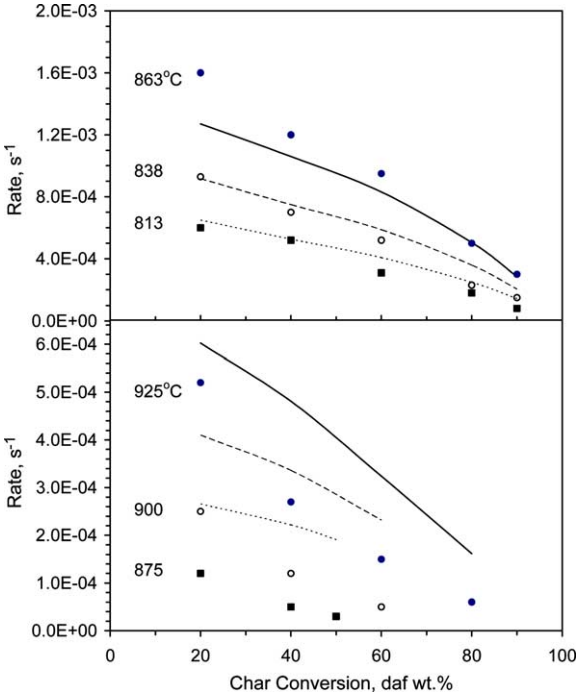

Fig. 21. Predicted (curves) and reported (data points) gasification rate vs. extent of char conversion for a hv bituminous char (upper) under 1.2 MPa steam and temperatures of (● and solid line) 863, (○ and dashed line) 838, and (■ and dotted line) 813 °C; and (lower) under 0.15 MPa steam and 0.045 MPa H_2, at (● and solid line) 925, (○ and dashed line) 838, and (■ and dotted line) 813 °C [15].

gasification alone, CBK/G accurately predicts the rate as a function of char conversion at all three temperatures, indicating the combined annealing mechanism and random pore model can represent the rate variations during conversion within useful quantitative tolerances. However, the default activation energy E_7 is slightly too low, so that the rates at 863 °C were slightly underpredicted and those at 813 °C were slightly overpredicted. The predicted reductions in the rate with char conversion under H_2O/H_2 are accurate, but the magnitudes of all rates were overpredicted at all temperatures. Since the predicted rates without H_2 inhibition are accurate, this flaw suggests that the default values of A_{60}/A_{70} and A'_{60}/A_{70} are unsuitable for this coal.

4.2.3. WVU dataset

At West Virginia University, a North Dakota lignite and Washington subbituminous, with carbon contents of 69.9 and 72.6 daf wt%, respectively, were gasified in a PTGA at 800–1200 °C under 76% steam at 0.78 MPa [16]. The mean particle size was 178 μm. Whole coal samples were first pyrolyzed in the PTGA at 100–1000 °C/s to the specified gasification temperature, then gasified in steam. The char conversion histories for lignite gasification are evaluated in

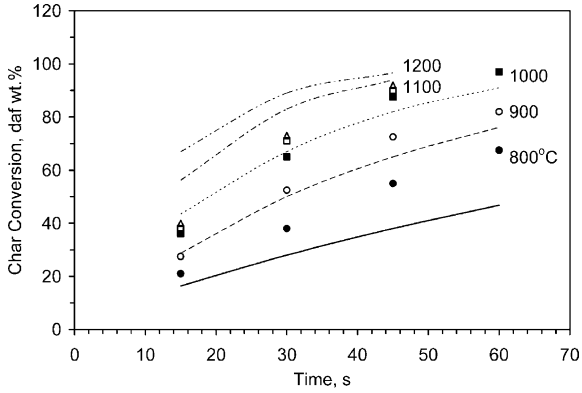

Fig. 22. Predicted (curves) and reported (data points) conversion histories for North Dakota lignite char gasification at 0.78 MPa under 76% H_2O at (● and solid line) 800, (○ and dashed line) 900, (■ and dotted line) 1000, (□ and dotted-dashed line) 1100, and (△ and double dotted-dashed line) 1200 °C [16].

Fig. 22. The comparisons of the conversion histories over the entire temperature range suggested that the activation energy E_7 assigned for this coal is slightly high. There are overpredictions for shorter times, especially for the first measurement time at the two hotter temperatures. This suggests that the assigned ψ_0 value of 4.6 in the random pore model is too high for this low rank coal.

A parity plot for char conversion for subbituminous gasification under 76% H_2O at 0.44–1.46 MPa from 1000 to 1400 °C appears in Fig. 23. All conversion data were seriously underpredicted at 0.44 MPa, and overpredicted at 1.46 MPa, suggesting that the pressure effect was overestimated by CBK/G for this coal. In fact, this subbituminous coal exhibited very little pressure dependence, which is very unusual according to Yang et al. [16]. It is worth noting that these poor predictions at 0.44 and 1.46 MPa made

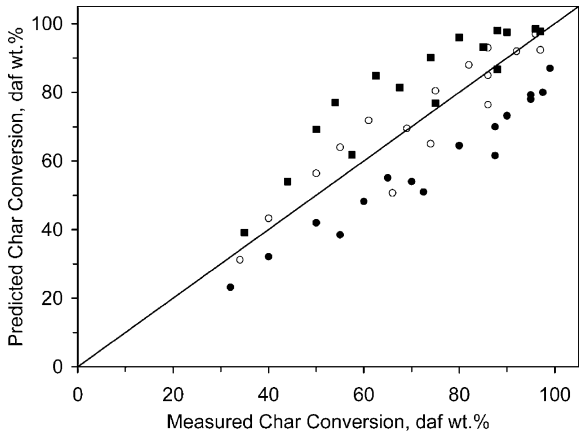

Fig. 23. Parity plot for conversion of Wash. subbituminous char gasification at (●) 0.44, (○) 0.78, and (■) 1.46 MPa and 1000, 1100, 1200, 1300, and 1400 °C under 76% H_2O in a PTGA [16].

disproportionate contributions to the SEE value of 11.4 daf wt% for the conversion predictions in the whole database.

4.2.4. EUT dataset

The group at Eindoven University of Technology tested El Cerejon, Gottelborn and Polish coals in a WMR [17]. The carbon contents of these coals were 83.6, 79.7 and 79.1 daf wt%, respectively. The reactor imposed a heating rate of 1600 °C/s to temperatures between 1227 and 1550 °C, at 0.1–1.5 MPa, with CO_2 levels between 2.5 and 100%. The mean particle size was 90.5 μm. Before the gasification experiments, char was first prepared in a drop tube furnace at 1400 °C for 250 ms. Fig. 24 evaluates the extents of char conversion for El Cerejon char at 1.5 MPa in 2.5% CO_2 and at various temperatures. The predictions at 1317 and 1467 °C are within experimental uncertainty throughout. At 1227 °C, the model overpredicted conversions, and at 1497 °C, it underpredicted them. This indicates that the activation energy assigned for El Cerejon is too low. The predicted conversion histories for Gottelborn and Polish bituminous chars at 1500 °C and 0.1 MPa in Fig. 25 are very accurate due to the combined annealing mechanism and random pore model incorporated in CBK/G.

4.2.5. AAU dataset

Gasification tests at Åbo Akademi University, Finland, used seven coals of rank from brown coal to bituminous with sizes of 100–150 μm [18]. Chars were prepared under an inert atmosphere for 300 s under the same conditions as those for gasification tests. Gasification rates were measured in a PTGA operated at 900 and 1000 °C at 0.1, 1.0 and 2.5 MPa with constant CO_2 and CO levels of 15 and 5%, respectively. The mean gasification rate over the entire conversion process was assigned.

As seen from Fig. 26, the measured rates at 900 °C with all chars except Gardanne and Rhenish brown char increase

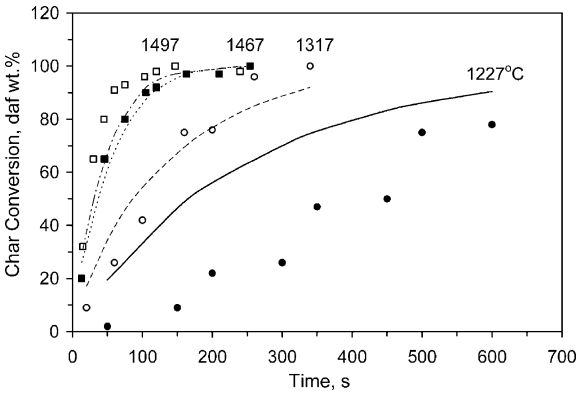

Fig. 24. Predicted (curves) and measured (data points) char conversion histories of El Cerejon bituminous char at (● and solid line) 1227, (○ and dashed line) 1317, (■ and dotted line) 1467, and (□ and dotted-dashed line) 1497 °C and 1.5 MPa with 2.5% CO_2 in a WMR [17].

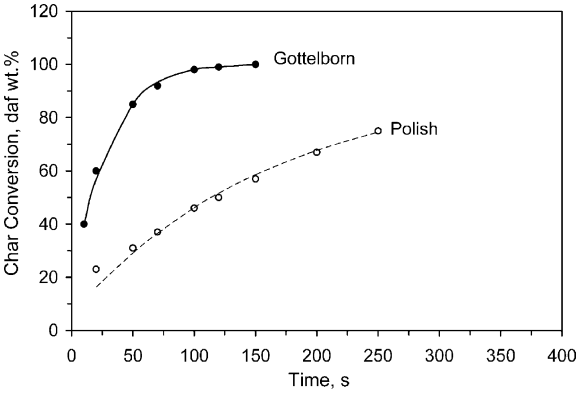

Fig. 25. Predicted (curves) and measured (data points) char conversion histories for (● and solid line) Polish and (○ and dashed line) Gottelborn chars at 1500 °C and 0.1 MPa pure CO_2 in a WMR [17].

for progressively higher pressures to 1.0 MPa, then stay the same. All the measured rates at 1000 °C are insensitive to pressure variations, but those for Ill.#6, Gardanne, and Rhenish brown char actually decrease at the highest test pressure. In contrast, the predictions for all chars at both temperatures display increasing rates for pressures to 1.0 MPa, and hardly any pressure effect for higher pressures. In general, the predicted pressure effect is too strong, and the assigned activation energies for all coals were slightly low.

Among these seven coals, Rhenish brown coal has the fastest gasification rate, whereas Westerholt bituminous char has the slowest. All the hv bituminous chars—Gottelborn, Kiveton Park, Westerholt and Polish—have essentially the same gasification rate.

4.2.6. ECUCT datasets

Our database includes two datasets from the East China University of Chemical Technology [19,20]. Tests reported by Sha et al. used Xiao Long Tan lignite char (68.3% C daf) with a size of 420–840 μm that was prepared under N_2 at 900 °C. The gasification rates were measured in a PTGA at 0.1 and 3.1 MPa at 850 and 900 °C. Fig. 27 evaluates the mean reaction rates in mixtures of $H_2O/CO/H_2$ and CO_2/CO. The gasification rates first increase as pressure was increased, but the pressure effect saturates for higher pressures. The pressure dependence is slightly overpredicted for gasification under CO_2/CO, and is slightly underpredicted for $H_2O/CO/H_2$. The assigned best-fit A_{70} is $5.6\times10^5\ s^{-1}$ for Xiao Long Tan.

The second dataset from ECUCT reported by Ma et al. [20] characterized steam gasification of Jincheng anthracite (92.5% C daf) of size 0.45–1.0 mm in a fixed bed reactor. Prior to the gasification tests, the char sample was prepared under N_2 at 5 °C/min and held for 2 h. Gasification tests were performed at 868–1096 °C and at 0.1–1.42 MPa. Fig. 28 evaluates the gasification rates as a function of char conversion under 1.0 MPa of H_2O at various reaction

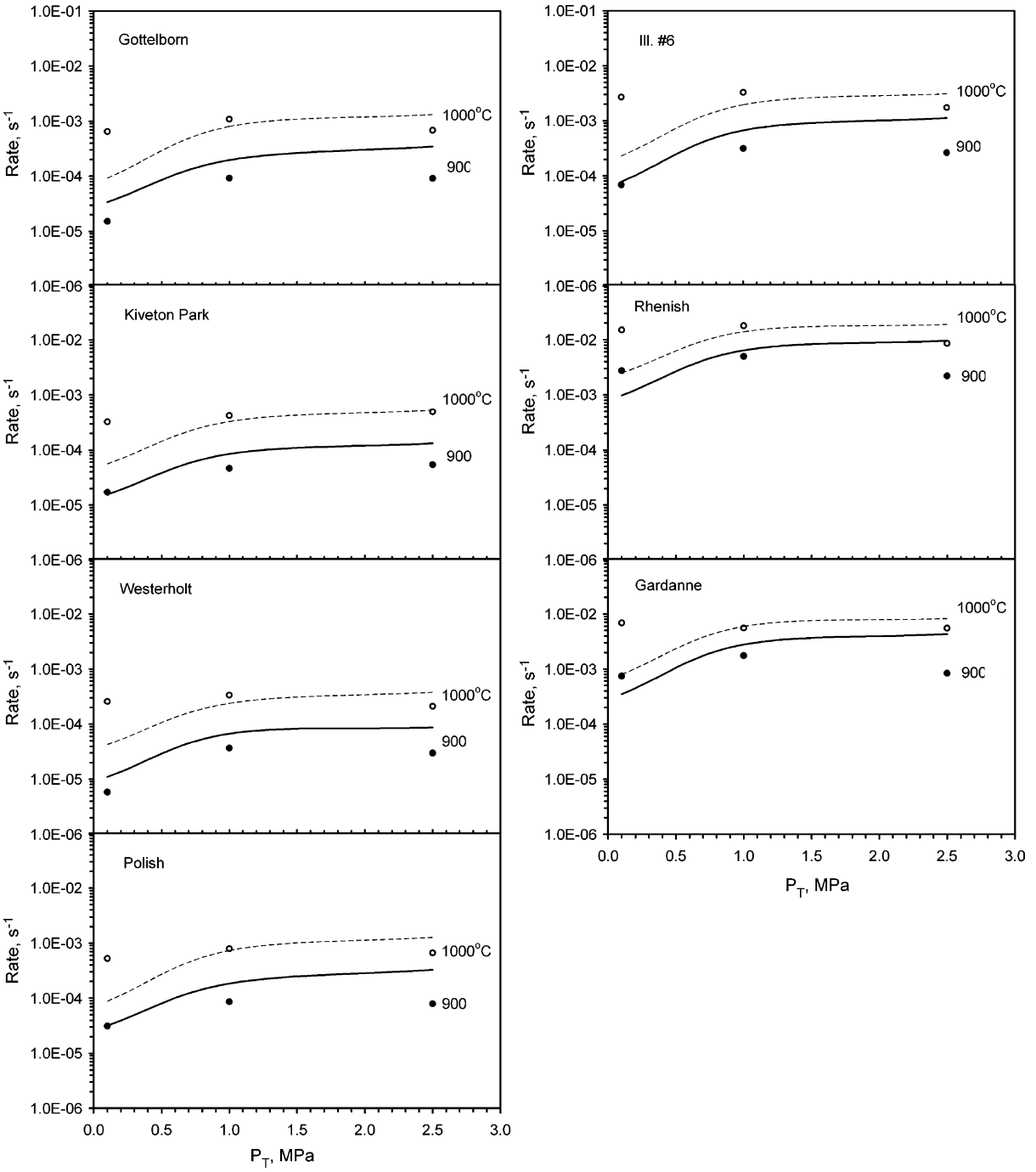

Fig. 26. Predicted (curves) and measured (data points) gasification rates for seven coal chars at (● and solid line) 900 and (○ and dashed line) 1000 °C in 15% CO_2 and 5% CO at various pressures [18].

temperatures. The predictions correctly depict the continuous decrease in the rates at all temperatures, and are within experimental uncertainty throughout all conversion levels.

As seen from Fig. 29, the pressure dependence of the rates at 20% conversion at 950 °C was accurately predicted. These rate profiles were obtained under pure steam at pressures of 0.1, 0.21, 0.47, 0.83 and 1.42 MPa. The predictions also correctly display decreasing rates at all pressures, but the absolute magnitudes for the predicted rates at high conversion levels are too high at elevated

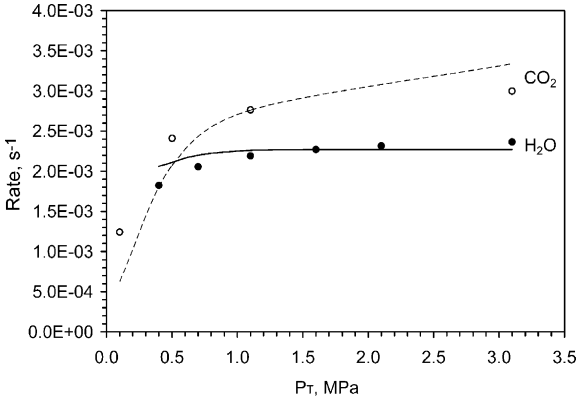

Fig. 27. Predicted (curves) and measured (data points) rates of Xiao Long Tan lignite char gasification at (● and solid line) 850 °C in 80% H_2O, 10% H_2, and 10% CO, and at (○ and dashed line) 900 °C in 90% CO_2 and 10 CO % [19].

pressures. This flaw worsens for progressively higher pressures to 0.47 MPa. A ψ parameter of 4.6 is probably unsuitable for this high rank coal.

4.2.7. IGT dataset

Western Kentucky bituminous was gasified at the Institute of Gas Technology [21]. The char was prepared at atmospheric pressure by heating at 6 °C/min to the temperatures in the gasification tests, which were 926, 982 and 1038 °C, for 30 min. The char particle size was varied between 350 and 850 μm. Gasification tests were performed in a PTGA from 0.4 to 2.8 MPa under steam, steam/H_2 and synthesis gas mixtures. The mean reaction rates were evaluated over the entire char conversion history.

As seen from Fig. 30, the measured gasification rates for steam gasification were independent of pressure, because even the lowest pressure in this test series is at the threshold

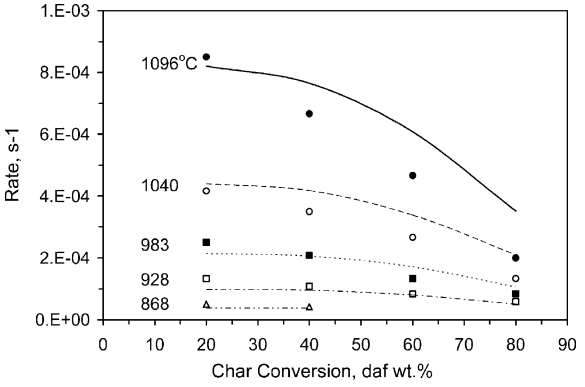

Fig. 28. Predicted (curves) and measured (data points) reaction rate profiles for Jincheng anthracite under 0.1 MPa steam at (● and solid line) 1096, (○ and dashed line) 1040, (■ and dotted line) 983, (□ and dotted-dashed line) 928, and (△ and double dotted-dashed line) 868 °C [20].

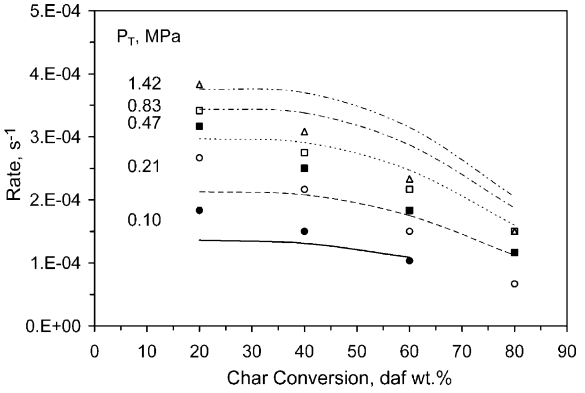

Fig. 29. Predicted (curves) and measured (data points) gasification rates vs. conversion for Jincheng anthracite at 950 °C under pure H_2O at (● and solid line) 0.1, (○ and dashed line) 0.21, (■ and dotted line) 0.47, (□ and dotted-dashed line) 0.83, and (△ and double dotted-dashed line) 1.42 MPa [20].

for negligible pressure effects seen in other datasets. Only the run at 0.4 MPa and 1098 °C is below the threshold and the measured rate does abide by the expected tendency for increasing rates for higher pressures in this pressure range. The measured rates in steam/H_2 mixtures were also independent of pressure. The predicted rates for steam

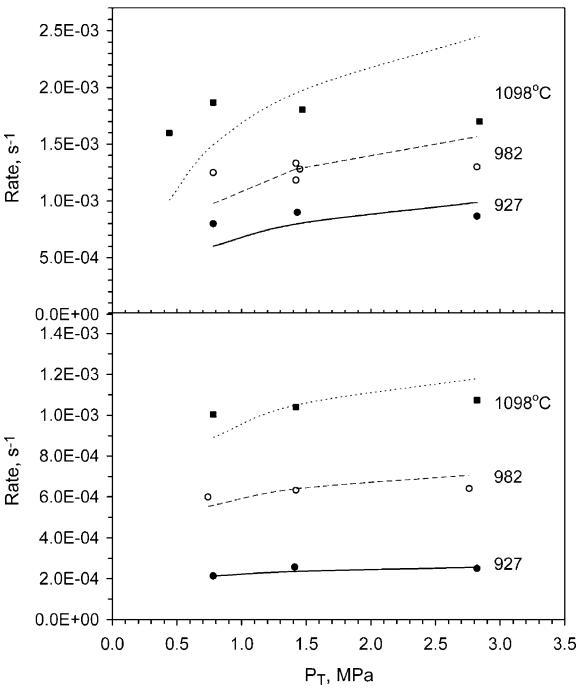

Fig. 30. Predicted (curves) and measured (data points) gasification rates for Kentucky bituminous char at (● and solid line) 927, (○ and dashed line) 982, and (■ and dotted line) 1098 °C under (upper) 50% H_2O or (lower) 50% H_2O and 50% H_2 in a PTGA [21].

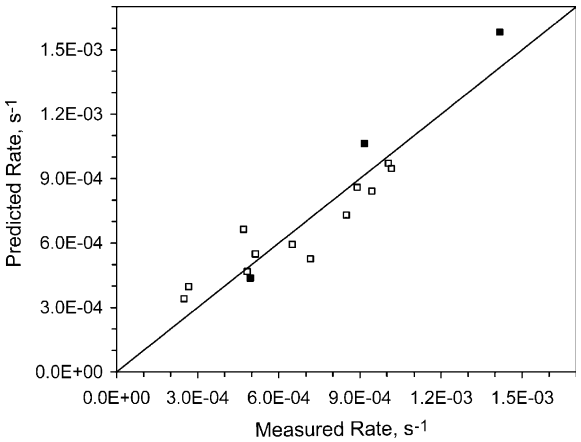

Fig. 31. Parity plot for gasification rates of Kentucky bituminous char under (■) 70% H_2O and 30% H_2 at 1.4 MPa, and (□) in synthesis gas at various pressures and temperatures in a PTGA [21].

gasification show a stronger pressure dependence for all temperatures. The predicted pressure effect for gasification in steam/H_2 mixtures is nearly consistent with the data.

Fig. 31 shows the parity plot for the gasification rates in a 70:30 mixture of H_2O/H_2 and in synthesis gas at various temperatures and pressures as in Table 6. The rates for both the H_2O/H_2 mixtures and the synthesis gas are predicted within useful quantitative tolerances.

4.2.8. UT dataset

The University of Tokyo dataset involves three subbituminous and an anthracite [22]. The gasification rates were measured in a PTGA at 850 °C under CO_2 partial pressures from 0.02 to 2.5 MPa. The char samples were prepared under N_2 at 1000 °C/min to 900 °C in a fluidized bed and held for 5 min. Fig. 32 evaluates the initial CO_2 gasification rates. The measured rates increase by up to a factor of six when the CO_2 pressure was increased to

Table 6
Operating conditions for char gasification in synthesis gas [21]

Run no.	T_P (°C)	P (MPa)	X_{CO2} (%)	X_{H2O} (%)	X_{CO} (%)	X_{H2} (%)
1	982	1.45	4.1	51	6.1	38.8
2	982	2.82	7.7	50.4	11.9	30
3	982	0.78	8.1	50.5	11.4	30
4	982	0.78	13	40.6	19	27.4
5	982	2.82	13	39.4	19.3	28.3
6	1038	1.41	4.3	51	6	38.7
7	1038	1.45	8.1	50.4	11.5	30
8	1038	1.43	7.4	51.3	11.2	30.1
9	1038	2.82	8.3	52	10.8	28.9
10	1038	0.78	8.9	50	11.4	29.7
11	1038	0.78	15.2	40.3	17.2	27.3
12	1038	1.46	13.3	40	17.2	29.5

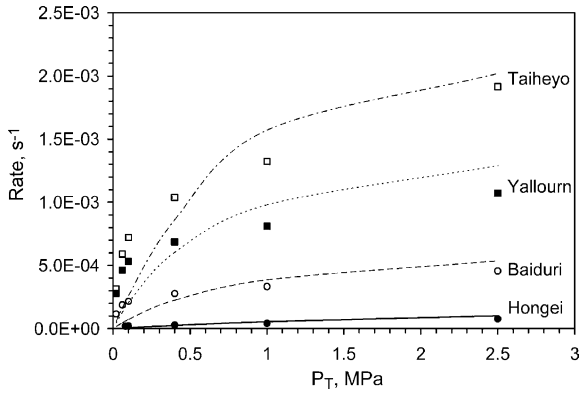

Fig. 32. Initial CO_2 gasification rates of (● and solid line) Hongei, (○ and dashed line) Baiduri, (■ and dotted line) Yallourn, and (□ and dotted-dashed line) Taiheyo at 850 °C in a PTGA [22].

2.5 MPa. This pressure effect was the same for Yallourn and Baiduri, very similar for Taiheyo except at the lowest test pressures, and stronger for Hongei. The only unusual feature in the data is that the pressure effect did not saturate at the highest test pressures. The predicted pressure effect is the same for all char types, and slightly stronger than any of the observed effects. Sensitivity analysis on the rate expression in Eq. (11) attributes the overprediction of pressure effects to a low value for the rate of CO_2 adsorption.

The predicted rank dependence is consistent with the data at pressures above 1.0 MPa, in so far as the gasification rate of the anthracite char is at least an order of magnitude slower than those for the rest. The rates at low pressures were underpredicted for all four coals. The rates for the Baiduri char are also slower than for both subbituminous chars, in accord with the data. These three rate profiles do not correlate with carbon content, so minerals probably play important roles.

4.2.9. CSIC dataset

The dataset from Consejo Superior de Investigaciones Cientificas involves CO_2 gasification of a Spanish lignite with 76.0 daf wt% carbon [23]. Char was made at atmospheric pressure in N_2 for 2 h at the same temperatures as those in the gasification tests. The char particle size ranged from 100 to 200 μm. Gasification was performed in a fluidized bed reactor from 800 to 1000 °C under either pure CO_2 or mixtures of CO_2 and CO in proportions from 88.5:11.5 to 54:46. Fig. 33 evaluates the initial gasification rates vs. pressure at 1000 °C for two mixture compositions. Under pure CO_2, the measured gasification rate increases for progressive increases in pressure, and the effect saturates for pressures over 1.0 MPa, as expected. This pressure dependence was accurately predicted by CBK/G. In a mixture of CO_2 and CO, the rate decreases for higher pressures due to the enhanced inhibiting effect of CO for increasing CO partial pressures. This feature is qualitatively evident in the predictions across the entire pressure range. However,

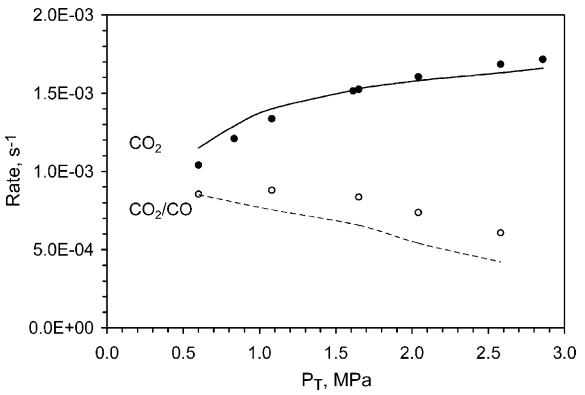

Fig. 33. Predicted (curves) and measured (data points) gasification rates for a Spanish lignite char at 1000 °C (● and solid line) under pure CO_2 and (○ and dashed line) in CO_2/CO mixtures of various proportions in a fluidized bed reactor [23].

the magnitudes were slightly underpredicted, indicating an inappropriate default value of A'_{40}/A_{70} for this coal.

4.2.10. CRIEPI dataset

The gasification rates of a Newlands bituminous char (82.5 daf wt% C) were measured in a PDTF at the Central Research Institute for the Electric Power Industry [24] at 1100–1500 °C and 0.2–2 MPa. The char was prepared in N_2 in an atmospheric DTF at 1400 °C for 3 s, then gasified in either CO_2 or steam. In one test series, the pressure was fixed at 0.5 MPa while the CO_2 or the H_2O mole fraction was varied. In the other, pressure and either the CO_2 or H_2O mole fraction was varied, so that the CO_2 and H_2O partial pressures were uniform at 0.5 and 0.02 MPa, respectively.

The initial gasification rates at 1300 °C for both CO_2 and H_2O appear in Fig. 34a. The predicted acceleration of the rate for progressively higher CO_2 levels is within experimental uncertainty over the full test range. The predicted reaction order with respect to CO_2 partial pressure decreases from unity to zero for progressively higher CO_2 mole fractions, in accord with the measured CO_2 gasification rates. For the same levels of these gasification agents, steam gasification rates are as much as five times faster than the CO_2 gasification rates at 1300 °C and 0.5 MPa.

The gasification rates for Newlands char at 1300 °C at uniform partial pressures of CO_2 and H_2O appear in Fig. 34b. The measured H_2O gasification rates increased by almost 50% when the pressure was increased from 0.2 to 2.0 MPa, which is difficult to explain. The CO_2 rates were essentially constant from 0.5 to 2.0 MPa, as expected. The model predicts almost the same gasification rates for both agents for this test series, because pressure variations, per se, have almost no impact. This prediction is confirmed by the CO_2 gasification rates within a slightly underpredicted magnitude. But the CBK/G prediction is inconsistent with the steam gasification rate data.

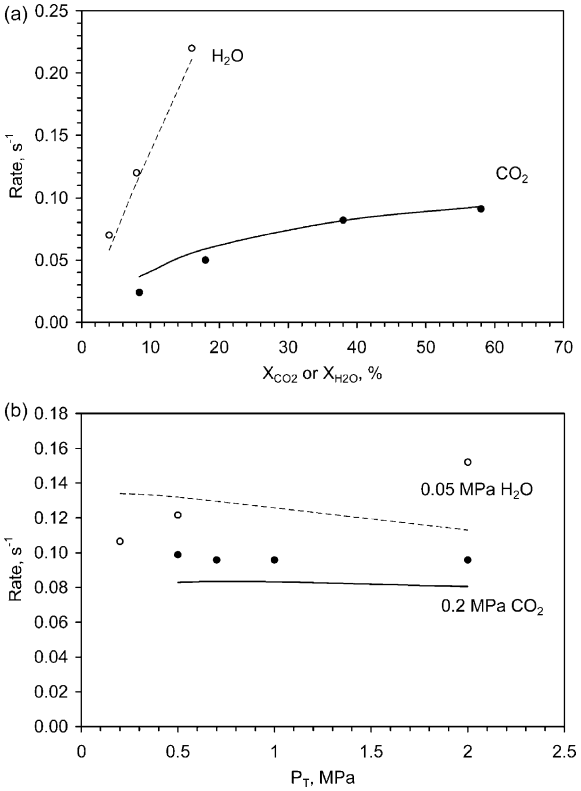

Fig. 34. (a) Predicted (curves) and measured (data points) initial gasification rates for Newlands bituminous char at 1300 °C, 0.5 MPa and various mole fractions of (● and solid line) CO_2 and (○ and dashed line) H_2O in a PDTF [24]. (b) Predicted (curves) and measured (data points) gasification rates for Newlands bituminous char at 1300 °C and fixed partial pressures of (● and solid line) CO_2 and (○ and dashed line) H_2O in a PDTF [24].

4.2.11. KEPRI dataset

At the Korean Electric Power Research Institute, an Indonesian subbituminous char (70% C daf) was characterized in a PDTF at gas temperatures of 900–1400 °C, CO_2 partial pressures of 0.1–0.5 MPa and pressures of 0.5–1.5 MPa [25]. The coal particle size was 45–64 μm, and the char was prepared in the PDTF in N_2 at 1400 °C for 600 ms. Fig. 35a evaluates the char conversion histories at 1.0 MPa under 20% CO_2 at various gas temperatures. The char conversion increased for hotter gas temperatures, as expected. The model predictions closely match the measurements at all four gas temperatures.

At face value, the measured conversion histories in Fig. 35b for various pressures at uniform CO_2 partial pressure indicate a significant pressure effect. Indeed, the reaction time needed to achieve a specified extent of conversion increased for progressively higher pressures. The times needed for 90% char conversion were 2.8, 3.3, 4.2, and 5.5 s at 0.5, 0.7, 1.0, and 1.5 MPa, respectively. The reason for this trend was already given in Section 2.3.2. Normally

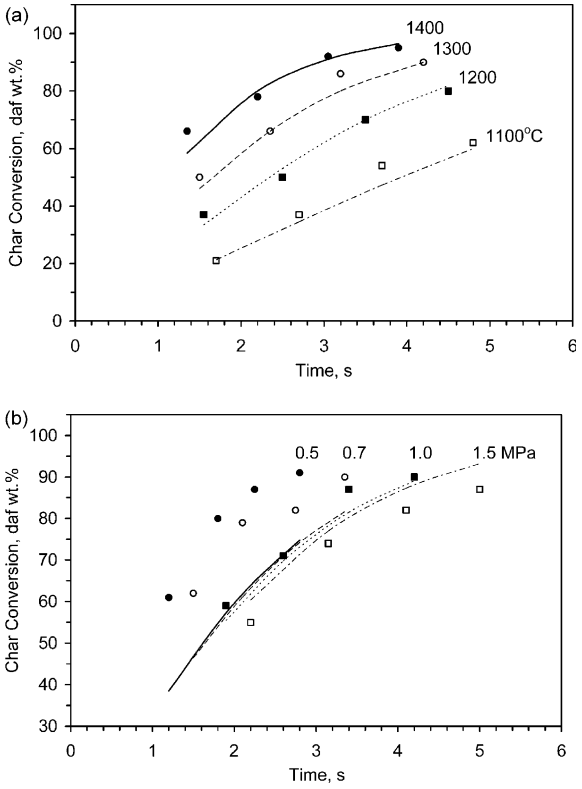

Fig. 35. (a) Predicted (curves) and measured (data points) conversion histories for Roto subbituminous chars at 1.0 MPa in 20% CO_2 at (● and solid line) 1400, (○ and dashed line) 1300, (■ and dotted line) 1200, and (□ and dotted-dashed line) 1100 °C in a PDTF [25]. (b) Predicted (curves) and measured (data points) conversion histories of Roto subbituminous chars at 1300 °C, a fixed CO_2 partial pressure of 0.2 MPa and (● and solid line) 0.5, (○ and dashed line) 0.7, (■ and dotted line) 1.0, and (□ and dotted-dashed line) 1.5 MPa in a PDTF [25].

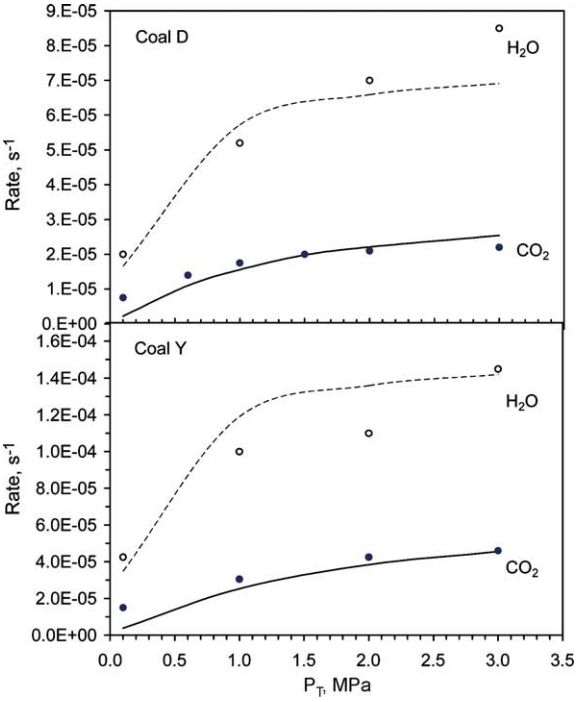

Fig. 36. Predicted (curves) and measured (data points) gasification rates for (upper) Coal D and (lower) Coal Y at (● and solid line) 900 °C in pure CO_2, and (○ and dashed line) 850 °C in pure steam in a PTGA [26].

a pore diffusion rate is independent of pressure because the pressure dependence in the reactant concentration cancels the inverse proportionality to pressure in the diffusivity. But since the partial pressure of the gasification agent was uniform in these tests, the diffusivity determines the pressure dependence in the transport rate, which would tend to diminish the overall gasification rate at progressively higher pressures, as was observed. These dependencies are included in CBK/G, and the predictions in Fig. 35b display the correct tendency. But the magnitude of this pressure effect is seriously underpredicted.

4.2.12. CRC dataset

The gasification rates of two Australian chars from bituminous Coal D with 82.5 daf wt% C and anthracite Coal Y with 90.6% C were measured in either CO_2 or steam in a PTGA at the University of Newcastle [26]. The chars were prepared in N_2 at atmospheric pressure at a heating rate of 10 °C/min and held for 3 h. CO_2 gasification was characterized at 900 °C for CO_2 pressures of 0.1–3.0 MPa, and steam gasification was measured at 850 °C under pure steam over the same pressure range. The rates were measured at a carbon conversion of 10%.

The measured CO_2 gasification rates for both Coal D and Coal Y exhibited similar pressure dependencies in Fig. 36. The steam gasification rates also increased with steam pressure, but the rate dependence decreased for higher steam pressures. Under the same pressures, the steam gasification rate is about 3–4 times that of CO_2 rates, even though the temperature of steam gasification was about 50 °C lower. The pressure dependence of steam gasification for both coal chars was slightly underpredicted at pressures above 1.0 MPa, but was otherwise accurate. The steam gasification rates for Coal Y were overpredicted at moderate pressures. Both the pressure dependence and the magnitude of CO_2 gasification rates were predicted within experimental uncertainty for both Coal D and Y.

4.3. Discussion

This section evaluates the predicted impacts of the operating conditions and interprets the assigned coal rank dependencies of the rate parameters in CBK/G.

4.3.1. Predicted impacts of the operating conditions

Whereas most of the data evaluations were satisfied within useful quantitative tolerances, many cases exhibited significant quantitative discrepancies. Indeed, no single aspect of the predictions was universally consistent with the data, primarily because data on the same aspect of gasification are not necessarily consistent over a broad range of coal quality. The predicted pressure dependence was generally confirmed in the data evaluations, except for the case with the Washington subbituminous in the WVU dataset [16], and with the Roto subbituminous in the KEPRI dataset [25]. Similarly, the predicted temperature dependence was confirmed, except for the case with El Cerejon in the EUT dataset [17]. Neither the predicted pressure dependence nor the predicted temperature dependence was consistent with the data for any of the coals in AAU dataset [18]. These poor predictions make disproportionate contributions to the overall SSE values of char conversion and gasification rates. If excluded, the SEE for conversion predictions drops to 8.8 daf wt%, and the SEE for rate predictions decreases to $\pm 16\%$ uncertainty.

CBK/G correctly predicts faster gasification rates for progressively higher CO_2 partial pressures, with an acute sensitivity at lower pressures and saturation to an asymptotic limit at higher pressures. From a quantitative standpoint, the numbers of cases with overpredicted, accurate, and underpredicted CO_2 dependencies were roughly the same, and the discrepancies were not confined to any segment of the rank spectrum. The performance regarding the order for steam pressure is the same.

However, one facet of these operating conditions was definitively established. The pair of cases in Fig. 37 evaluates the predictions for two versions of the surface reaction mechanism. In the ultimate version of CBK/G, steam and CO_2 gasification share a common surface oxide but the rates of the oxide desorption are different. This mechanism correctly predicts different asymptotic limits for each gasification agent, in accord with the data. But the predictions from the earlier version that applied the same desorption rate for both gasification agents are erroneous. In this particular pressure range, the gasification rates are inverted, such that the limiting CO_2 gasification rate appears to be much higher than the steam gasification limit at very high pressures. In fact, this mechanism yields the same limiting rate for both gasification agents at very high pressure, where desorption controls the overall gasification rates, at odds with the available data for the highest test pressures. This flaw could not be eliminated by adjusting any of the other rate parameters. Applying different desorption rates to the common surface oxide is a direct way to rectify this problem, although more complex surface kinetics could also be applied.

One could reasonably expect that the impact of pressure variations with fixed partial pressures of the gasification agents would be among the more straightforward aspects of the evaluations. CBK/G correctly predicted no pressure

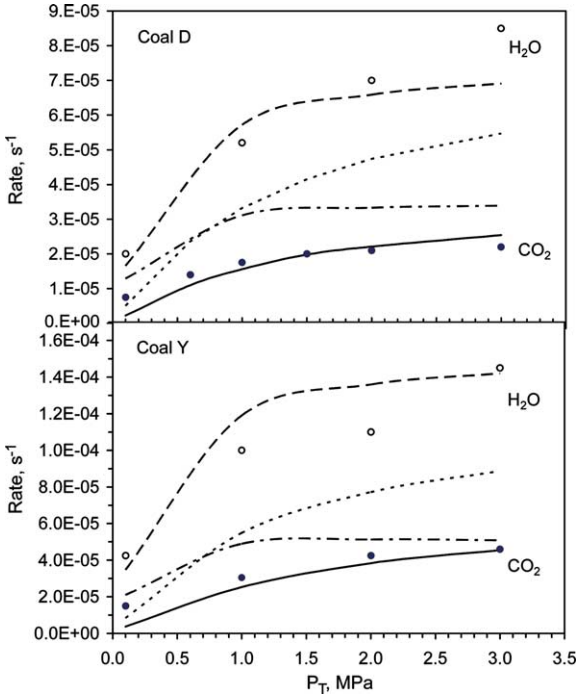

Fig. 37. Evaluations of gasification rates for (upper) Coal D and (lower) Coal Y at (●) 900 °C in pure CO_2, and (○) 850 °C in pure steam in a PTGA [26] for CBK/G (solid and dashed curves) and for a preliminary version with a common desorption rate for the surface oxide pool for CO_2 and steam gasification (dotted and dot-dashed curves).

effect under this constraint for CO_2 gasification at CRIEPI (cf. Fig. 34b). But the predicted reduction in the rate of steam gasification was at odds with the observed enhancement for higher operating pressures in the same system (cf. Fig. 34b). Also, the predicted reduction in the CO_2 gasification rate for higher pressures was much less than the reduction observed at KEPRI (cf. Fig. 35b). It is conceivable that CBK/G incorrectly predicted the gasification zone and, consequently, incorrectly predicted when the gasification rate becomes inversely proportional to pressure (for fixed concentration of the gasification agent). But rate enhancements for higher pressures are inconsistent with our postulated gasification kinetics, which are corroborated by the bulk of the database. Moreover, flow reactors impose slower gas heating rates at progressively higher pressures, due to the progressively greater sensible energy requirements of the flow. This factor should also be considered in the interpretations of data on this effect.

Only three datasets isolated the inhibiting effects of CO and H_2, which were generally consistent with the CBK/G predictions. These effects can be attributed to the rank-dependent correlations for A'_{40}/A_{70} and A'_{60}/A_{70} in Eqs. (40) and (42), respectively. But more data on a much wider variety of coals are needed to specify these rates within closer

tolerances. Similarly, only the dataset from IGT represents complete mixtures of CO_2, H_2O, CO and H_2. These cases are especially relevant to practical gasifiers, because they involve multi-step heterogeneous reactions, as well as shifting reactions in the gas phase. CBK/G with the option for equilibrated gas compositions accurately predicted these data, but many more datasets with such complex mixtures are needed for stringent model evaluations.

The seven evaluations of the temperature dependence in the gasification rates were satisfied within useful quantitative tolerances. But the nearly universal quantitative discrepancies suggest that the rank-dependent correlation for activation energy E_7 is an expedient substitute for data to specify this parameter on a sample-specific basis. Since mineral catalysis is probably the basis for most of the deviations from the correlation-based predictions, calibration data should be obtained over the temperature range of interest to specify this important parameter for each fuel sample.

The status of CBK/G's representation of the gasification rate as a function of carbon conversion is similar. The combination of the annealing mechanism and the random pore model impart the correct form to the predicted rate reductions with conversion, which were quantitatively perfect in at least one case (cf. Fig. 25). But the uniform default value for the ψ-parameter in the random pore model should be replaced with sample-specific values based on data, particularly for applications at low-to-moderate temperatures where the pore coalescence effects are comparable to the annealing effects.

4.3.2. Rank dependence of the rate parameters

In the data evaluations, the only parameter that was adjusted for each fuel sample was the frequency factor for surface oxide desorption during steam gasification, A_{70}. The best-fit values for A_{70} for each dataset appear in Fig. 38, where the abundance of ranks from subbituminous to bituminous reflects this bias in the database. The parameter assignments change in the mean by almost two orders of magnitude for subbituminous and hv bituminous coals, but the spread at any particular C-content is comparable. The smaller spread for lignites and low volatility coals appears to be an artifact of their poor representation in the database, although this remains to be established with additional testing.

The following linear correlation between $\log_{10}(A_{70})$ and coal rank was specified from the assigned A_{70} for all coals:

$$\log_{10}(A_{70}) = 0.1C_{daf} - 0.64 \quad (46)$$

where C_{daf} denotes the coal carbon content in daf wt%. There is a clear tendency for greater A_{70}-values for coals of progressively higher rank. (As illustrated in Fig. 39 below, this does not mean that the overall gasification rate increases with coal rank, because the activation energy E_7 also increases with coal rank according to Eq. (44).)

Several factors are responsible for this tendency and, more importantly, for the large variations among samples of the same nominal rank. Char preparation conditions affect a char's physical and chemical properties, but mineral catalysis has already been demonstrated to exert much larger effects on gasification rates [31]. Alkali and alkaline earth cations, especially Ca, K, and Na, are the most important inherent catalysts. Unfortunately, the mineral loadings in the coals were not reported for almost all the samples in the database, so mineral catalysis cannot be characterized in any quantitative way. The connections among the spread in the assigned A_{70}-values and mineral catalysis is the main reason that a one-point calibration is needed to make accurate predictions with CBK/G on a sample-specific basis. The range of test temperatures in our evaluation is moderate compared to entrained flow gasification conditions, and catalytic effects are more pronounced at

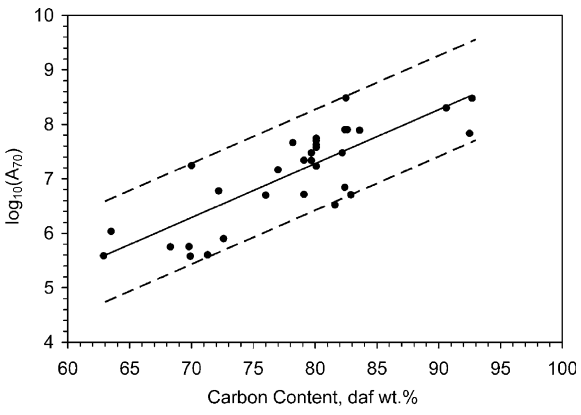

Fig. 38. Rank dependence of the assigned values for A_{70}. Solid circles denote the best-fit values for each coal. The solid line represents the correlation between A_{70} and a coal's carbon content. Dashed lines show the nominal spread.

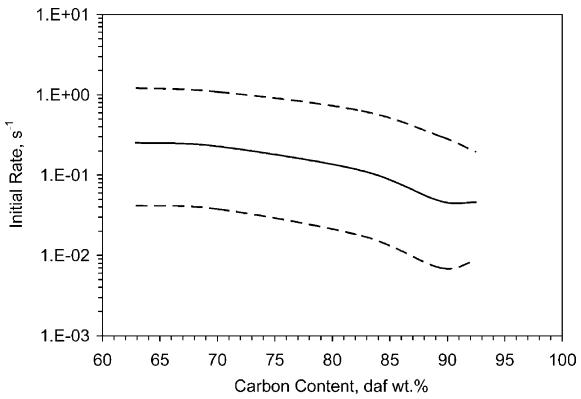

Fig. 39. (Solid curve) Rank dependence based on the correlation in Eq. (46) of the initial burning rate of a 90-μm particle injected into gases at 1400 °C within a 1200 °C EFR at 2.0 MPa with 10% CO_2, 30% H_2O, 10% CO and 10% H_2. (Dashed curves) Rates associated with the spread in A_{70}-values in Fig. 38.

lower temperatures. So the best calibration data will be in the temperature range for the ultimate application.

Fig. 39 illustrates the rank dependence in the gasification rates from the default parameter assignments in CBK/G for typical entrained-flow gasification conditions. It shows the predicted rank dependence of the initial gasification rates of chars from the entire rank spectrum. For chars of progressively higher rank, the nominal gasification rate decreases monotonically from 0.25 to 0.04 s^{-1}, due to the rank-dependent rate parameters (A_{70}, E_7, A_{40}/A_{70}, A_{60}/A_{70}, A'_{40}/A_{70} and A'_{60}/A_{70}). Note, however, that the variation over almost the entire rank spectrum is even less than the variation for any particular rank associated with the spread in the A_{70}-values in Fig. 38.

Consequently, the default correlations in Eqs. (39)–(44) and (46) can only depict the overall tendency in the initial gasification reactivity with coal rank, not the sample-specific gasification rates. CBK/G with the default correlations for its rate parameters should be regarded as a powerful tool for extrapolating across a wide domain of operating conditions, given sufficient measurements on the gasification of every coal of interest to specify the initial reactivity parameter, A_{70}. A one-point calibration for every sample, with either an extent of conversion or rate determination, is necessary to predict char gasification rates across a wide domain of operating conditions, although calibration data over the temperature range of interest is required to achieve the closest quantitative tolerances.

5. Practical applications

Two considerations pave the way for practical applications. First, it is not necessary to build CBK/G or any other comprehensive gasification mechanism into CFD or other complex engineering calculations, because we can analyze model predictions as we would analyze lab data to specify the parameters in simple rate expressions that will closely mimic the gasification behavior from the complete mechanism. Second, the enormous savings in time in using model predictions compared to lab testing opens up a multitude of opportunities for additional case studies, including broad domains of coal quality and process operating conditions. These advantages are illustrated further in the following section, beginning with the assignment of simplified rate laws. Case studies then survey gasification rates during the gasification of individual particles for wide ranges of coal quality and operating conditions. Finally, CBK/G is used to simulate the gasification of a coal suspension in a 1D entrained flow gasifier to illustrate some essential complexities that arise in engineering applications.

5.1. Global gasification rate expressions

Complex calculations like CFD implement rudimentary rate expressions for gasification. Usually *n*th-order power laws are used, in which the concentration of each gasification agent appears as a multiplicative factor raised to some fractional power. *n*th-Order rate laws that account for the inhibitors, CO and H_2, have not yet been reported, although more complex Langmuir–Hinschelwood-type forms have been used. The temperature dependence is expressed by the activation energy parameter in a rate constant of Arrhenius form. These expressions do not resolve the independent influences of intrinsic chemistry, transport, pore evolution, and deactivation, so they cannot possibly remain accurate over broad domains of the operating conditions. Nevertheless, some global rate expressions can accurately depict the gasification rate over a limited domain, provided that the parameters are specified properly. Under the best circumstances—which almost never arise in practice—the parameters can be assigned from a database compiled for the same operating conditions as the practical application. In practice, however, the user is usually left to determine how the kinetic parameters should be adjusted to extrapolate from a calibration domain to the operating domain, and for different coal samples. He or she can compile a database, consult an expert, or use a comprehensive mechanism to extrapolate. Here we illustrate extrapolations based on CBK/G.

It is always possible to identify the parameters in simple, global rate laws for gasification that will closely mimic the predictions from more sophisticated models like CBK/G. Here we illustrate the procedure with the single, *n*th-order reaction (SNOR) modified for inhibition by CO, but any simple rate expression can be analyzed in the same way. The modified SNOR for gasification by CO_2 is

$$R_{CO_2} = \vartheta R^0_{CO_2} = \vartheta \frac{A_{CO_2} \exp(-E_{CO_2}/RT) P^{n_{CO_2}}_{CO_2,S}}{1 + K_{CO} P_{CO,S}} \tag{47}$$

where $R^0_{CO_2}$ is the surface reaction rate not subject to annealing and physical evolution effects; ϑ is a factor to account for annealing and physical evolution effects to be defined further; A_{CO_2}, E_{CO_2} and n_{CO_2} are the pre-exponential factor, activation energy and reaction order for gasification by CO_2; K_{CO} is the rate constant for CO inhibition which is independent of temperature; and $P_{CO_2,S}$ and $P_{CO,S}$ are the instantaneous CO_2 and CO partial pressures (in atm) on the particle surface. Factoring the gasification rate into separate contributions for the primary concentration and temperature dependencies in $R^0_{CO_2}$ and for the annealing and physical evolution effects in ϑ is a convenient way to expand the domain of applicability of the rate expression. ϑ can be expressed as a simple polynomial decay to represent the joint impact of the main inhibitory mechanisms that decelerate the char gasification rate with conversion, including annealing, random pore evolution, and char density changes. ϑ will be expressed as a fifth-order polynomial regression.

Similarly, the modified SNOR for gasification by H_2O is

$$R_{H_2O} = \vartheta \frac{A_{H_2O} \exp(-E_{H_2O}/RT) P_{H_2O,S}^{n_{H_2O}}}{1 + K_{H_2} P_{H_2,S}} \quad (48)$$

and the SNOR for gasification by H_2 is

$$R_{H_2} = \vartheta A_{H_2} \exp(-E_{H_2}/RT) P_{H_2,S}^{n_{H_2}} \quad (49)$$

For situations where all the gasification agents are present, the overall gasification rate should be evaluated as the product of the rates in Eqs. (47)–(49).

In these rate laws, all parameters are adjustable constants that change with pressure, gas composition, temperature history and coal type, due to the inherent limitations. It is important to realize that their magnitudes have no mechanistic significance whatsoever, because such simple reaction rate expressions cannot possibly represent the numerous mechanisms that, in actuality, govern the kinetics of char gasification.

The parameters A, E, and n are usually assigned from laboratory test data. Instead, we use CBK/G to synthesize simulation 'data' that can subsequently be analyzed for rate parameters just like one would analyze test measurements. The goal is to specify rate parameters for the modified SFOR that are able to accurately describe the gasification rate over a complete gasification history as, for example, across an entrained-flow gasifier. Consequently, it is important that the ambient conditions applied to CBK/G to obtain a complete gasification history for the parameter assignments are as similar as possible to the ambient conditions in the application of interest. The procedure first evaluates the rate for a baseline extent of char conversion, then at a different temperature and different surface partial pressures of the reactant gases. A, E and n are assigned from the CBK/G-based rates by rearrangements of the modified SFOR expression.

For example, to specify a nominal rate of CO_2 gasification, we first specify the ambient conditions of interest, then use CBK/G to predict the extents of char conversion and the gasification rates throughout a complete gasification history. From the predicted gasification history, first evaluate the reaction rate $R^0_{CO_2}(1)$ and the surface conditions T_1, $P_{CO_2,1}$, $P_{CO,1}$ near the maximum extent of char conversion, up to 70%. Then assign the temperature range of interest with T_2, the temperature at the onset of char gasification in the CBK/G simulation, and obtain the reaction rate $R^0_{CO_2}(2)$, for surface conditions T_2, $P_{CO_2,1}$, and $P_{CO,1}$. Similarly, use CBK/G to evaluate rates $R^0_{CO_2}(3)$ and $R^0_{CO_2}(4)$ for $P_{CO_2,2} = 1.2P_{CO_2,1}$ and $P_{CO,2} = 0.3P_{CO,1}$, respectively, where the pair of the other surface conditions are at baseline values in both cases. Values for A_{CO_2}, E_{CO_2}, n_{CO_2} and K_{CO} are evaluated by rearrangement of the rate expression, Eq. (48), as follows:

$$E_{CO_2} = -\frac{\log_{10}(R^0_{CO_2}(2)/R^0_{CO_2}(1))}{(1/T_2 - 1/T_1)} \quad (50)$$

$$n_{CO_2} = \frac{\log_{10}(R^0_{CO_2}(3)/R^0_{CO_2}(1))}{\log_{10}(P_{CO_2 2}/P_{CO_2 1})} \quad (51)$$

$$K_{CO} = \frac{R^0_{CO_2}(1) - R^0_{CO_2}(4)}{(P_{CO_2} R^0_{CO_2}(4) - P_{CO_1} R^0_{CO_2}(1))} \quad (52)$$

$$A_{CO_2} = \frac{R^0_{CO_2}(1)(1 + K_{CO} P_{CO_1,S})}{\exp(-E_{CO_2}/RT_1) P^{n_{CO_2}}_{CO_2,S_1}} \quad (53)$$

This same analysis can be applied to gasification with H_2O and H_2.

The fifth-order polynomial correlation for the decay in the reaction rate with conversion is written as:

$$\vartheta = a_0 + a_1 X + a_2 X^2 + a_3 X^3 + a_4 X^4 + a_5 X^5 \quad (54)$$

where X is extent of char conversion and a_i ($i = 0$–5) denotes the regression coefficients. These coefficients are evaluated by fitting the product of the annealing factor, surface area factor (from the random pore model), and char density factor evaluated directly from the baseline CBK/G simulation. Generally, the accuracy is improved if two separate correlations are specified for extents of char conversion above and below 10%.

The performance of the method is illustrated in Fig. 40 for 1D entrained gasification of an hv bituminous coal under typical commercial conditions, as fully specified in Section 5.3, below. The partial pressures of H_2O, CO and H_2 change continuously throughout gasification, but the CO_2 concentration is uniform because steam gasification dominates under these conditions. The char conversion history based on the modified SNOR-assignment is compared to the original CBK/G predictions in the upper panel of Fig. 40. Notwithstanding the wide variations in the concentrations of the gasification agents, the agreement is nearly exact throughout the entire gasification history. The lower panel demonstrates the performance for an extrapolation for the same coal to a 10% increase in the O_2/coal flowrate and a 15% increase in the H_2O/coal flowrate from the baseline conditions. Even though the modified SNOR parameters determined for the baseline case were used in the simulation, the predicted char conversion history is very close to the CBK/G-based history. The minor underprediction for extents of char conversion from 40 to 80% would be inconsequential in most design studies.

5.2. Gasification of individual coal particles

The simulations in this section move the validated version of CBK/G toward the context of entrained coal gasification with several sensitivity studies on the overall impacts of coal rank, pressure and gas environment under typical entrained-flow gasification conditions. They are, however, restricted to the scale of isolated, individual particles. Suspension effects are illustrated in Section 5.3. The predictions in Fig. 41 illustrate the coal conversion,

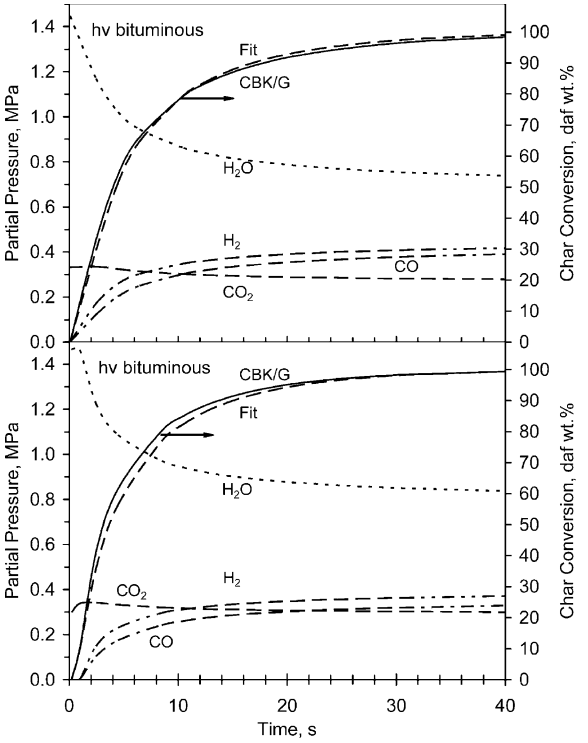

Fig. 40. Comparison of predicted char conversion histories from CBK/G (solid curve) and the modified SNOR rate assignments (dashed curve) for baseline entrained flow gasification (upper) and a case with increased O_2 and H_2O flowrates (lower) with an hv bituminous coal. The variations in the partial pressures of H_2O, CO_2, CO and H_2 also appear.

particle size, and density histories for three diverse coals along a uniform pressurized flow. These simulations were based on the proximate and ultimate analyses for representative subbituminous, hv bituminous and lv bituminous coals, and the default rate parameters in CBK/G.

Coal devolatilization is completed within 50 ms for these coals under such severe conditions, which is much shorter than the subsequent char gasification stage. So the devolatilization behavior is not apparent in these histories and will not be discussed because our characterization of coal quality impacts on devolatilization at elevated pressure was reported separately [2]. The extents of coal conversion due to devolatilization are 20% for the lv bituminous, 40% for the hv bituminous, and about 60% for the subbituminous. This factor, in conjunction with the slower gasification rate of the lv bituminous, is responsible for its significantly longer gasification time. This coal also swells to the largest size and has the lowest bulk char density. Conversely, the subbituminous has the smallest char size and the fastest gasification rate and, therefore, the shortest conversion time. The hv bituminous is intermediate in all aspects except for changes in bulk char density during the first 25 s. All gasification rates diminish continuously throughout

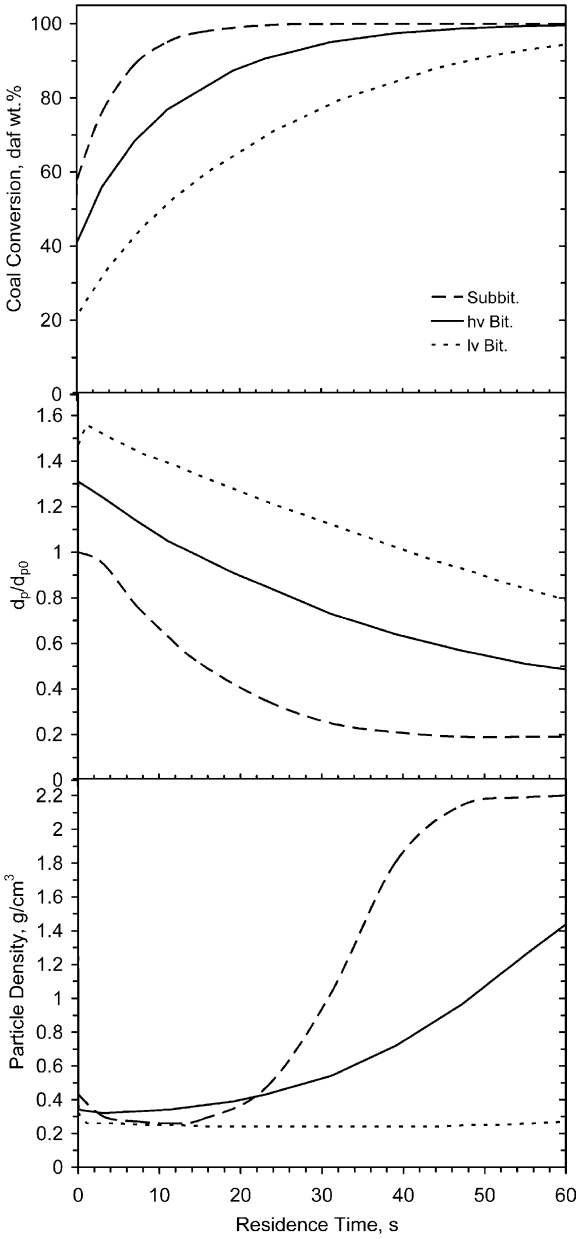

Fig. 41. Predicted coal conversion (upper), particle size (middle), and particle density (lower) of 90-μm subbituminous (dashed line), hv bituminous (solid line) and lv bituminous (dotted line) coals injected into 10% CO_2, 30% H_2O, 10% CO and 10% H_2 at 1400 °C and 2.0 MPa within a channel at 1200 °C.

gasification. The char density plummets during devolatilization, remains uniform throughout most of the gasification history, then surges during the latest stages of conversion to the much higher density of aluminosilicate-based ash.

Simulations in Fig. 42 for the hv bituminous coal illustrate the impact of pressure variations. The baseline operating conditions were specified in Fig. 41. The coal

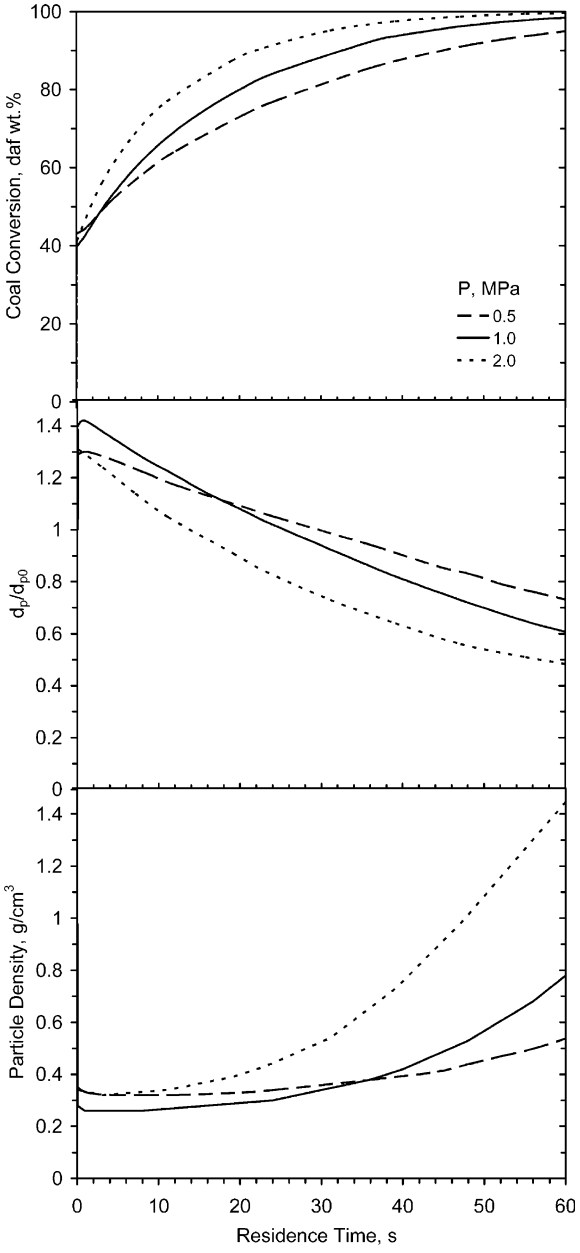

Fig. 42. Predicted coal conversion (upper), particle size (middle), and particle density (lower) of 90-μm hv bituminous coal injected into a 1200 °C flow with 10% CO_2, 30% H_2O, 10% CO and 10% H_2 at 1400 °C and at (dashed line) 0.5, (solid line) 1.0 and (dotted line) 2.0 MPa.

conversion due to devolatilization is about 42% at all three operating pressures, because ultimate devolatilization yields generally reach an asymptotic pressure limit below 1.0 MPa [2]. But increasing the pressure from 0.5 to 2.0 MPa significantly accelerates the char gasification rates, so that the ultimate coal conversion levels increase from 95.0 to 98.4 to 99.5 daf wt% as pressures was increased from 0.5 to 1.0 to 2.0 MPa, respectively. The swollen initial char size passed through a maximum at 1.0 MPa that is 40% larger than the coal particle size due to the pressure-dependent swelling correlation in CBK/G. The size diminished continuously throughout gasification under these operating conditions. Char particle densities were hardly affected by the pressure variations, except that the time scale for the asymptotic approach to the ash density varied with the gasification rate.

Fig. 43 shows the gasification histories under different gas environments for a fixed pressure of 2.0 MPa. The coal conversion levels due to devolatilization are the same under the three gas environments. The overall gasification rate increased only modestly when the concentrations of the gasification agents were doubled. But adding 10% of the inhibitors, CO and H_2, significantly retarded the gasification rate. Note especially that the impact of inhibitors is more significant than large changes to the concentrations of the primary gasification agents, yet inhibitors are routinely ignored in global gasification rate expressions applied in engineering calculations.

5.3. 1D gasification of coal suspensions

The simulations in the previous section isolate the impacts of coal quality and selected operating conditions on the gasification rates of individual particles under typical gasification conditions. But the gasification behavior of individual particles is only one facet of gasifier simulations, primarily for two reasons. First, the concentrations of the gasification agents in a gasifier are mostly determined by chemistry in the gas phase. Volatiles are first converted into secondary pyrolysis products, then reformed by partial oxidation into mixtures with CO_2, H_2O, CO, and H_2. Usually steam injection supplements the inherent concentrations, and char gasification adds additional carbon to the gas phase which continuously perturbs the gas compositions along the gasifier. Second, secondary volatiles pyrolysis converts a major portion of the volatiles into soot, which is another condensed phase that needs to be heterogeneously gasified. With hv bituminous coals, well over half the volatiles yield can be converted into soot, so this effect is definitely not negligible. Notwithstanding, we know of no analysis of gasification histories in the literature that recognizes the impact of soot on gasification rates throughout a gasifier. The simulations in this section illustrate both effects.

5.3.1. Simulation strategy

Our intention is to focus on the coupling among soot production, volatiles reforming, the concentrations of the gasification agents, and the resulting char gasification rates along a gasifier. For the sake of simplicity, the entrained-flow gasifier is rendered as a plug flow reactor with radially well-mixed coal particles and gas. The reactor is divided

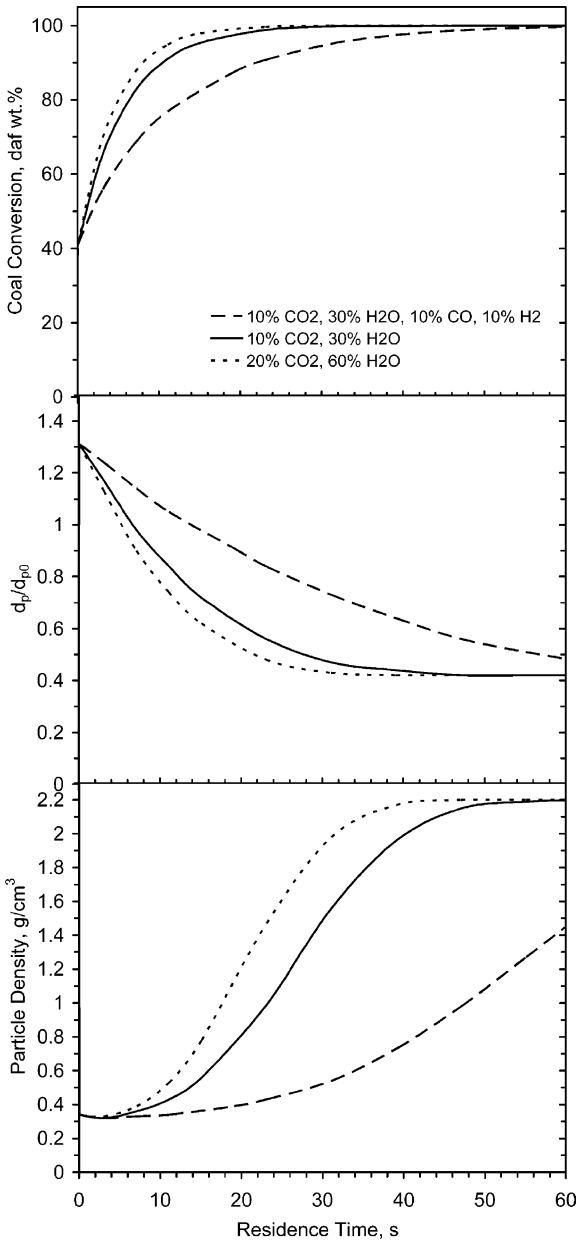

Fig. 43. Predicted coal conversion (upper), particle size (middle), and particle density (lower) of a 90-μm hv bituminous coal injected into a 1200 °C flow at 2.0 MPa with gases at 1400 °C with (dashed line) 10% CO_2, 30% H_2O, 10% CO and 10% H_2, and (solid line) 10% CO_2 and 30% H_2O and (dotted line) 20% CO_2 and 60% H_2O.

into two stages. The first stage sustains simultaneous coal devolatilization, volatiles combustion, and char oxidation; the second stage sustains char gasification. The first stage is fired with O_2, N_2, and coal, and steam is injected at the inlet to the second stage.

The key aspects of the first stage performance are the extents of conversion of char and soot, which are determined in a competition among these fuels with the gaseous volatile fuel compounds for the available O_2. The outcome of this competition can only be predicted from realistic kinetics for this multiphase combustion process. This aspect of the simulations is well beyond the scope of this paper. Suffice to say that our ChemNet™ post-processing methodology accommodates extensive elementary reaction mechanisms for chemistry in the gas phase and on soot in combination with CBK/E for char oxidation [56,57]. FLASHCHAIN® was used to predict the distributions of secondary pyrolysis products, including soot; a 15-step mechanism described soot oxidation by O_2, O, and OH and recombination of H and OH; and a 444-step reburning mechanism described the gas phase chemistry.

In the 1D gasifier simulations, ChemNet™ determines the input gas compositions, char properties, and loading of char and soot that enter the gasification stage. CBK/G was then used to simulate the gasification stage with an equilibrium submodel for gas compositions. Gas compositions were updated continuously for the addition of carbon to the gas phase via char and soot conversion. The soot gasification rate was assigned with CBK/G in the kinetically controlled limit (zone I), based on the limiting value of A_{70} for the highest rank coal in the database, due to its small size and lack of mineral cations.

5.3.2. Coal analyses and operating conditions

Typical properties for a subbituminous, hv and lv bituminous coals were used to evaluate the coal quality impacts on gasifier performance. The proximate and ultimate analyses are listed in Table 7. The nominal size was 55 μm. With reference to Texaco gasifier conditions [58], the gasifier was simulated at 2.0 MPa with the coal

Table 7
Coal analyses and feedrates used in the entrained flow gasification simulations

	Subbituminous	hv Bituminous	lv Bituminous
Coal analyses			
Moisture (ad wt%)	0.1	0.0	1.6
VM (ad wt%)	36.4	28.7	15.7
Ash (ad wt%)	5.0	13.8	5.1
FC (ad wt%)	58.5	57.5	77.8
C (daf wt%)	73.9	82.5	89.4
H (daf wt%)	5.6	5.1	4.4
O (daf wt%)	19.0	10.5	3.1
N (daf wt%)	1.1	1.5	2.2
S (daf wt%)	0.6	0.4	0.9
Feedrates			
Coal feedrate (g/s)	62	62	62
O_2/coal (g/g s)	0.853	0.870	1.022
N_2/coal (g/g s)	0.367	0.367	0.367
Steam/coal (g/g s)	1.070	1.300	1.325
SR (–)	0.8	0.8	0.8

feedrates and the mass ratios of O_2/coal, steam/coal and N_2/coal in Table 7. Whereas the coal feedrates and the N_2/coal ratio were fixed, O_2/coal and steam/coal ratios were perturbed to maintain overall SR values of 0.8 for all coals.

The gas temperature histories in practical gasifiers would be different for these coals, because the devolatilization rates and yields, and the char oxidation and gasification rates are strongly rank dependent. However, for sake of simplicity, a common gas temperature history was imposed for all coals. In the first stage, the gas temperature history peaked at 1500 °C; the second stage was isothermal at 1200 °C. A uniform wall temperature of 1400 °C was imposed for all simulations. The first stage residence time was fixed at 100 ms, at which time the steam was instantaneously mixed into the flow.

5.3.3. Simulation results

Fig. 44 shows the formation histories of char, soot and O_2, CO_2, H_2O, CO and H_2. Note that char, soot, and H_2 appear on the finer *y*-axis on the right. The fine scale for the first 100 ms resolves the competition for O_2 in the first stage, and the succeeding scale covers almost 40 s of gasification in the second stage.

In the first stage, devolatilization occurs while the suspension is heated at rates approaching 10^5 °C/s. The yields of total volatiles and soot are strongly rank-dependent: These respective values are 51.2 and 13.6 daf wt% for the subbituminous; 36.7 and 14.1% for the hv bituminous; and 18.7 and 9.7 for the lv bituminous. Oxygen is consumed within 15 ms with the subbituminous, and within 30 ms with both bituminous coals in the oxidation of gaseous fuel compounds, soot, and char. The apportioning of O_2 among these fuels is also rank dependent. The fastest burning chars have the lowest extents of soot conversion, because faster char oxidation reduces the O_2 level more, and because the burning rates of all soots are the same. That is, chars with the fastest burning rates compete more effectively for the available O_2 than soot, as expected [59]. Consequently, the extents of char and soot burnout in the first stage are 39.2 and 10.8% for the subbituminous; 42.1 and 33.6% for the hv bituminous, and 53.9 and 33.8% for the lv bituminous. Note, however, that the extents of char oxidation are not consistent with the intrinsic char oxidation rates, which diminish for chars of progressively higher rank. The reason is that neither of the condensed fuel species competes effectively for O_2 with the gaseous fuel compounds. The yields of gaseous volatiles diminish from 37.6 to 22.6 to 9.0% among these three coals, so there is much more O_2 available to burn out the bituminous chars in the first stage, especially with the lv bituminous.

While O_2 is being consumed, the levels of CO_2 and H_2O increase. But as soon as O_2 disappears, water gas shifting converts substantial portions of the CO_2 into CO, and the CO_2 levels pass through maxima in the first stage. There is much less shifting into H_2 (on a mass basis) so the H_2O levels appear to remain at plateaus during the final 60 ms of the first stage. These variations follow the tendency expected for the variation in the SR values of the gas phase only. Initially, the SR of the gas phase is nominally infinite, because no fuel compounds are present. Fuels are added, first, during devolatilization, then during the oxidation of char and soot into CO, which reduces SR. Once SR becomes substoichiometric, CO and H_2 become appreciable. At the outlet to the first stage, the subbituminous generates the most H_2O and the least CO_2, as well as the most soot.

Steam injection at the inlet to the second stage perturbs the CO_2 level and, especially, the H_2 level to higher values, at the expense of CO. In this way, the variations in the steam injection strengths counteract the variations in the gas compositions from the first stage among the different coals. Immediately after steam injection, the gas compositions for these coals are much more uniform than at the end of the first stage.

The rank-dependence in the char gasification rates is clearly apparent in the different conversion times for the different coals. The subbituminous is completely converted in less than 15 s, whereas the hv bituminous char is not quite converted after 37 s and more than 10% of the lv bituminous char remains at the outlet. Clearly, the rank dependence in the char gasification rates is an essential aspect of gasifier simulation. Furthermore, the levels of H_2O, H_2, and CO vary widely throughout the bulk of char conversion. Only the CO_2 level is fairly uniform throughout, because the gasification rate for this agent is negligible compared to steam's. Steam concentrations decay in tandem with the reduction in the char level while the levels of CO and H_2 rise. So only gasification kinetics for complex gas mixtures are directly relevant to gasifier performance evaluations. Outlet gas compositions are fairly similar with these three coals, except for more CO with the lv bituminous. Finally, despite the very high levels of H_2O and CO_2 throughout, the soot levels from all three coals are reduced by less than half during gasification. Soot is the predominant source of unburned carbon emissions with the subbituminous and hv bituminous, but contributes less than a third of the carbon emissions from the lv bituminous.

Despite the simplistic geometry and flow pattern, the 1D gasifier simulation illustrates several essential facets of gasification chemistry under relevant operating conditions. The ultimate yields of gaseous volatiles, soot, and char from devolatilization are strongly rank dependent. A competition for the available O_2 among gaseous fuels, soot, and char determines the extents of conversion of soot and char into the second stage. This competition is responsible for significant differences among the gas compositions, soot loadings, and char levels into the second stage. However, steam injection eliminates most of the variations in gas composition. From a practical standpoint, the most important characteristics from a first gasifier stage are the residual levels of char and soot. Char levels increase and soot levels decrease with coals of progressively higher rank.

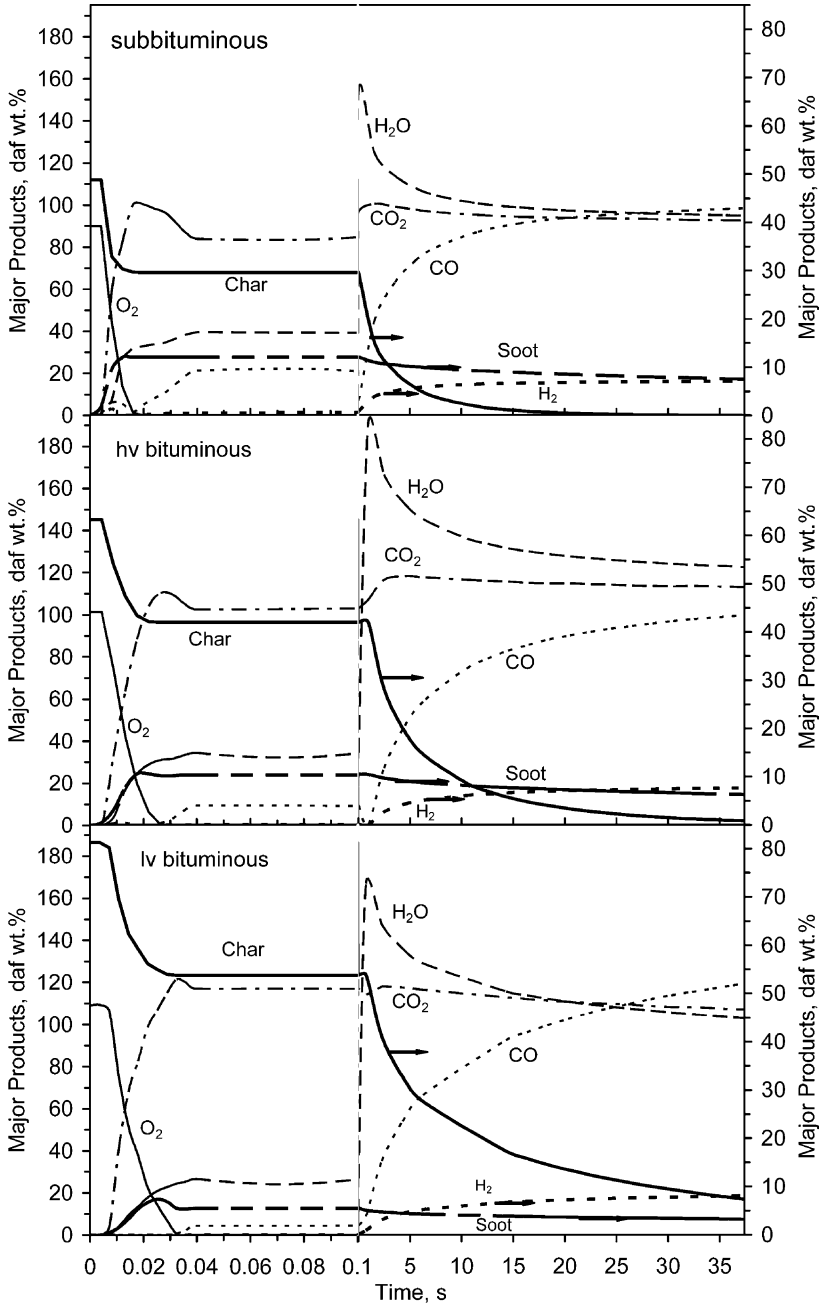

Fig. 44. Predicted levels of (bold solid line) char, (bold dashed line) soot, (solid line) O_2, (dotted-dashed line) CO_2, (dashed line) H_2O, (dotted line) CO and (bold dashed line) H_2 of (upper) subbituminous, (middle) hv bituminous and (lower) lv bituminous in a 1D gasifier flow at 1400 °C and 2.0 MPa and an overall SR of 0.8. The levels of char, soot, and H_2 appear on the right scale. Steam was injected at the end of the first stage, after 100 ms.

Gasification kinetics alone determine the behavior in the second stage. The rank dependence of gasification rates is the determining factor for extents of char conversion at the outlet. But soot gasification kinetics will determine the unburned carbon emissions for all but the highest rank fuels.

6. Summary and recommendations

6.1. Summary

The database reported in English on coal char gasification at elevated pressures covers the relevant domain of

operating conditions for current and advanced technology, except for CO_2 sequestration processes that operate at 6–8 MPa. Four hundred and fifty-three independent tests with 28 different coals characterized pressures from 0.02 to 3.0 MPa, CO_2 and steam mole percentages from 0 to 100%, CO and H_2 levels to 50%, gas temperatures from 800 to 1500 °C, and most of coal rank spectrum. Only a handful of cases characterized inhibition by CO and H_2, and only a single dataset represented the complex mixtures of H_2O, CO_2, CO, and H_2 that arise in practical applications. Also, low rank and low volatility coals were underrepresented. The most commonly reported measurements were either extents of conversion or the gasification rate, which are equally represented. Generally, particle temperatures and particle sizes were not measured.

The database exhibits several trends that are essential for rational design of pressurized coal gasification technologies. With uniform gas composition, gasification rates increase for progressively higher pressures, especially at lower pressures. Whereas the pressure effect saturates at the higher pressures with bituminous chars, no saturation is evident with low-rank chars. With fixed partial pressures of the gasification agents, the pressure effect is much weaker. It may only arise under operating conditions where pore diffusion is the rate controlling mechanism. Gasification rates increase for progressively higher gas temperatures. In general, gasification rates diminish for coals of progressively higher rank, but the data exhibit this tendency only for ranks of hv bituminous and higher. Mineral catalysis becomes more significant than the generic rank dependence for low-rank chars, so the carbon content of the parent coal no longer correlates this portion of the rank dependence.

CBK/G incorporates a combined oxidation/gasification mechanism involving the three surface reactions for char oxidation in CBK/E plus four reactions for gasification by CO_2, H_2O, CO and H_2. Rate reductions due to annealing were applied uniformly to all reactions, consistent with the current gaps in understanding how annealing affects individual reactions in the set. Whereas the same surface oxide is postulated for steam and CO_2 gasification, different desorption rates had to be applied to depict the distinctive limiting values of these gasification rates at very high pressures. The oxide pools for combustion and gasification were regarded as independent for analogous reasons. Film diffusion resistances are included but unimportant under practical gasification conditions. Effectiveness factors account for intraparticle transport resistances through the bulk combustibles and through an ash layer during the latest stages, providing the impetus for automatic shifts between zones I and II. The annealing mechanism, in conjunction with a random pore model at the lowest gasification temperatures, depicts the diminishing gasification rate throughout char conversion.

CBK/G includes 13 rate parameters. Almost all of them were assigned from reported values or in preliminary calculation sweeps through the database. Rank dependencies were applied to the frequency factors in the forward and reverse rates of production of a surface oxide during gasification by both CO_2 and steam, and to the frequency factor and activation energy for oxide desorption during steam gasification. The ratio of the oxide desorption rates during CO_2 and steam gasification is a function of temperature. Only A_{70}, the frequency factor for oxide desorption during steam gasification, was specified to fit the database.

This strategy was designed to determine whether CBK/G could be applied to a wide domain of operating conditions after a one-point calibration. Whereas most of the data evaluations were satisfied within useful quantitative tolerances, many cases exhibited significant quantitative discrepancies. No single aspect of the predictions was universally consistent with the data, primarily because data on the same aspect of gasification are not necessarily consistent over a broad range of coal quality. Notwithstanding, implementation of this strategy demonstrates the following capabilities:

- The SEE values are 11.4 daf wt% for predicted extents of char conversion and $\pm 22.7\%$ for gasification rate predictions.
- The predicted pressure and temperature dependencies were generally confirmed in the data evaluations. But the nearly universal quantitative discrepancies in the temperature dependence suggest that the rank-dependent correlation for activation energy E_7 is an expedient substitute for data to specify this parameter on a sample-specific basis.
- CBK/G correctly predicts faster gasification rates for progressively higher CO_2 partial pressures, with an acute sensitivity at lower pressures and saturation to an asymptotic limit at higher pressures. From a quantitative standpoint, the numbers of cases with overpredicted, accurate, and underpredicted CO_2 dependencies were roughly the same, and the discrepancies were not confined to any segment of the rank spectrum. The performance regarding the order for steam pressure is the same.
- Equal desorption rates for a common surface oxide pool for steam and CO_2 gasification yields the same limiting rate for both gasification agents at very high pressure, where desorption controls the overall gasification rates. This behavior is at odds with the available data for the highest test pressures. Applying different desorption rates to the common surface oxide is a direct way to rectify this flaw, although more complex surface kinetics could also be applied.
- CBK/G correctly predicted no pressure effect for fixed CO_2 partial pressures for CO_2 gasification at CRIEPI (cf. Fig. 34b). But it could not interpret the reported enhancement in the rate of steam gasification for higher operating pressures in the same system, or the large

pressure effect in the CO_2 gasification rates for higher pressures observed at KEPRI.

- The predicted inhibiting effects of CO and H_2 were generally consistent with the reported behavior, but more data on a much wider variety of coals is needed to specify the rates associated with this effect within closer tolerances. Indeed, inhibition is as important as very substantial changes in the H_2O and CO_2 concentrations.
- CBK/G in conjunction with equilibrated gas compositions accurately described the lone dataset on complex mixtures with all the most important gasification agents, but many more such datasets are needed for stringent model evaluations.
- The combination of the annealing mechanism and the random pore model impart the correct form to the predicted rate reductions with conversion. But the uniform default value for the ψ-parameter in the random pore model should be replaced with sample-specific values based on data, particularly for applications at low-to-moderate temperatures, where the pore coalescence effects are comparable to the annealing effects.

The assigned values of A_{70} increase for coals of progressively higher rank, albeit within variations of almost two orders of magnitude among samples of the same nominal rank. The smaller spread in values for lignites and low volatility coals appears to be an artifact of their poor representation in the database, although this remains to be established with additional testing. Whereas several factors could rationalize the large variations among samples of the same nominal rank, uncharacterized catalysis by alkali and alkaline earth cations is the most likely reason. The connections among the spread in the assigned A_{70}-values and mineral catalysis is the main reason that a one-point calibration is needed to make accurate predictions with CBK/G on a sample-specific basis. Consequently, the best calibration data will span the temperature range for the ultimate application.

With the default parameter assignments, CBK/G predicts that nominal gasification rates decrease monotonically for chars of progressively higher rank. However, the predicted variation over almost the entire rank spectrum is even less than the variation for any particular rank associated with the spread in the assigned A_{70}-values. Consequently, the default correlations for the rate parameters can only depict the overall tendency in the gasification reactivity with coal rank, not sample-specific gasification rates. CBK/G with the default correlations for its rate parameters should be regarded as a powerful tool for extrapolating across a wide domain of operating conditions, given sufficient measurements on the conversion of every coal of interest to specify the initial reactivity parameter, A_{70}.

The rank dependence in the nominal gasification rates is a determining factor for the gasification history in a practical gasifier, but there are additional factors to consider. The rank dependence in ultimate devolatilization yields is as strong at elevated pressure as at atmospheric pressure [2]. Consequently, the residual amount of char to be gasified varies widely among samples of even the same nominal rank, although the nominal tendency is for larger char yields from coals of progressively higher rank. Also, char particles swell the most at moderate pressures, especially bituminous coals, although char particle size exerts a minor impact on gasification rates under practical operating conditions.

Two additional aspects are essential for accurate simulations of gasifier performance. First, the concentrations of the gasification agents in a gasifier are mostly determined by chemistry in the gas phase. Volatiles are first converted into secondary pyrolysis products, then reformed into mixtures with CO_2, H_2O, CO, and H_2. Steam injection supplements the inherent concentrations, and char gasification adds additional carbon to the gas phase that continuously perturbs the gas compositions along the gasifier. Second, secondary volatiles pyrolysis converts a major portion of the volatiles into soot, which also needs to be heterogeneously gasified. With hv bituminous coals, well over half the volatiles yield can be converted into soot, so this effect is definitely not negligible. Notwithstanding, we know of no analysis of gasification histories in the literature that recognizes the impact of soot on gasification rates throughout a gasifier.

The interplay among all these factors was illustrated with a 1D gasifier simulation to identify the most important ones. As expected, the ultimate yields of gaseous volatiles, soot, and char from devolatilization are strongly rank dependent, as are char burning rates. Consequently, there were significant differences among the gas compositions, soot loadings, and char levels into the second stage with different coals. However, steam injection eliminates most of the variations in gas composition. Hence, the most important characteristics from a first gasifier stage are the residual levels of char and soot. Char levels increased and soot levels decreased with coals of progressively higher rank. Gasification kinetics alone govern the behavior in the second stage. The rank dependence of gasification rates is the determining factor for extents of char conversion at the outlet. But soot gasification kinetics will determine the unburned carbon emissions for all but the highest rank fuels. Only gasification kinetics for gas mixtures with widely variable levels of H_2O, H_2, and CO are directly relevant to gasifier performance evaluations.

6.2. Recommendations

The following additional laboratory testing is needed to improve CBK/G's predictive capabilities:

1. Laboratory studies involving large and diverse sample sets (>20 coals) gasified under standard conditions in 1D laboratory flow devices are needed to develop improved correlations between coal properties and the initial char gasification reactivity. Loadings of alkali and

alkaline earth cations must be monitored for all samples to resolve catalysis from inherent rank effects. The gasification measurements should be supported by detailed characterizations of the composition and morphology of char, to identify the factors that actually determine a char's initial gasification reactivity.
2. Lab testing, in general, should be diverted away from cases with a single gasification agent to (i) thoroughly characterize inhibition by CO and H_2 for a wide variety of coals and (ii) to characterize the complex mixtures of gasification agents that arise in practical gasifiers.
3. Gasification rates for coal-derived soot should be directly monitored. Readily available aerosol recovery methods should be applied to coal gasification tests to independently monitor extents of soot gasification [60].
4. The coupling among secondary volatiles pyrolysis, gas phase chemistry, and the conversion of char and soot needs to be characterized with tests that monitor all the major gaseous species plus char and soot throughout gasification at realistic suspension loadings.

In addition, the following two theoretical developments will significantly improve design tools for commercial gasifiers:

1. CBK/G should be used to specify the parameters in the simpler heuristic rate expressions deployed in CFD simulations that mimic the predictions from the complete model. New global rate expressions need to be developed to depict inhibition by CO and H_2 and the diminishing gasification rates for progressively higher extents of char conversion.
2. Simplified quasi-global mechanisms and rate expressions need to be developed for (i) volatiles reforming into CO_2, CO, H_2, and H_2O; (2) the extents of burnout of char and soot in air- or O_2-blown gasifier stages. One expedient approach would develop simpler, quasi-global schemes from reported elementary reaction mechanisms for the gas phase chemistry.

Acknowledgements

The initial development of gasification mechanisms by Professor Robert Hurt at Brown University is gratefully acknowledged.

References

[1] Lin SY, Hirato M, Horio M. The characteristics of coal char gasification around ash melting temperatures. Energy Fuels 1994;8:598–606.
[2] Niksa S, Liu G-S, Hurt H. Coal conversion submodels for design applications at elevated pressures. Part I. Coal devolatilization and char oxidation. Prog Energy Combust Sci 2003;29(5):425–77.
[3] Wall TF, Liu G-S, Wu H-W, Roberts DG, Benell KE, Gupta S, et al. The effect of pressure on coal reactions during pulverized coal combustion and gasification. Prog Energy Combust Sci 2002;28:405.
[4] Fletcher TH, Zeng D, Clark M, Hecker WC. Properties of coal chars produced at elevated pressures and high heating rates. Proceedings of the 12th international conference on coal science, Cairns, Queensland, Australia; November 2–6, 2003.
[5] Tang L, Gupta R, Sheng C, Wall TF. Single particle approach of CPD model to predict high temperature VM yields of coal. Proceedings of the 12th international conference on coal science, Cairns, Queensland, Australia; November 2–6, 2003.
[6] Yu J, Strezov V, Lucas J, Liu G-S, Wall TF. A mechanistic study on char structure evolution during coal devolatilization—experiments and model predictions. Proc Combust Inst 2002;29:467–73.
[7] Yu J, Strezov V, Lucas J, Wall TF. Swelling behaviour of individual particles in the single particle reactor. Fuel 2003; 15–17:1977–87.
[8] Yu J-L, Lucas J, Strezov V, Wall T. Swelling and char structures from density fractions of pulverized coal. Energy Fuels 2003;17:1160–74.
[9] Messenböck RC, Dugwell DR, Kandiyoti R. CO_2 and steam-gasification in a high-pressure wire-mesh reactor: the reactivity of Daw Mill coal and combustion reactivity of its chars. Fuel 1999;78:781–93.
[10] Messenböck RC, Dugwell DR, Kandiyoti R. Coal gasification in CO_2 and steam: development of a steam injection facility for high-pressure wire-mesh reactors. Energy Fuels 1999; 13(1):122–9.
[11] Messenböck RC, Paterson NP, Dugwell DR, Kandiyoti R. Factors governing reactivity in low temperature coal gasification. Part 1. An attempt to correlate results from a suite of coals with experiments on maceral concentrates. Fuel 2000;79:109–21.
[12] Lim J-Y, Chatzakis IN, Megaritis A, Cai H-Y, Dugwell DR, Kandiyoti R. Gasification and char combustion reactivities of Daw Mill coal in wire-mesh and hot-rod reactors. Fuel 1997; 76(13):1327–35.
[13] Zhuo Y, Messenbock R, Collot A-G, Megaritis A, Paterson N, Dugwell DR, et al. Conversion of coal particles in pyrolysis and gasification: comparison of conversions in a pilot-scale gasifier and bench-scale test equipment. Fuel 2000;79:793–802.
[14] Megaritis A, Messenböck RC, Chatzakis IN, Dugwell DR, Kandiyoti R. High-pressure pyrolysis and CO_2 gasification of coal maceral concentrates: conversions and char combustion reactivities. Fuel 1999;78:871–82.
[15] Weeda M, Abcouwer HH, Kaptejn F, Moulijn JA. Steam gasification kinetics and burn-off behaviour for a bituminous coal derived char in the presence of H_2. Fuel Process Technol 1993;36:81.
[16] Yang RYK, Lee IC, Raghunathan K, Peng FF, Jiang WD. Kinetics of high temperature and pressure char-steam reaction in coal gasification. NTIS No. DE87001088, Department of Chemical Engineering, University of West Virginia, Morgantown, WV; 1986.
[17] Moors JHJ. Pulverized char combustion and gasification at high temperatures and pressures. PhD Dissertation, Eindoven Tech. Univ., The Netherlands; 1998.

[18] Zevenhoven R, Hupa M. Characterization of solid fuel at pressurized fluidized bed gasification conditions. Proceedings of the 23rd international technical conference on coal utilization and fuel systems, March 9–13, 1998, Clearwater, FL, USA; 1998. p. 81–92.
[19] Sha XZ, Chen YG, Cao J, Yang YM, Ren DQ. Effects of operating pressure on coal gasification. Fuel 1990;69:293.
[20] Ma ZH, Zhang CF, Zhu ZB, Sun EL. A study on the intrinsic kinetics of steam gasification of Jincheng coal char. Fuel Process Technol 1992;31:69.
[21] Goyal A, Zabransky RF, Rehmat A. Gasification kinetics of Western Kentucky bituminous coal char. Ind Eng Chem Res 1989;28:1767.
[22] Nozaki T, Adschiri T, Fujimoto K. Coal char gasification under pressurised CO_2 atmosphere. Fuel 1992;71:213.
[23] Adánez J, Miranda JL, Gavilan JM. Kinetics of a lignite-char gasification by CO_2. Fuel 1985;64:801.
[24] Kajitani S, Hara S, Matsuda H. Gasification rate analysis of coal char with a pressurized drop tube furnace. Fuel 2002;81:539–46.
[25] Ahn DH, Gibbs BM, Ko KH, Kim JJ. Gasification kinetics of an Indonesian subbituminous coal char with CO_2 at elevated pressure. Fuel 2001;80:1651–8.
[26] Roberts DG, Harris DJ. Char gasification with O_2, CO_2, and H_2O: effects of pressure on intrinsic reaction kinetics. Energy Fuels 2000;14:483–9.
[27] Li S, Sun R. Kinetic studies of a lignite char pressurised gasification with CO_2, H_2 and steam. Fuel 1994;73:413.
[28] Li S, Xiao X. Gasification reactivity of three Chinese coal chars with steam at elevated pressure. Fuel 1993;72:1351.
[29] Abichandani JS, Deradourian C, Gannon RE, Stickler DB, Woodroffe JA. Pressure effects on steam pyrolysis of coal. Fuel Process Technol 1988;18:133–46.
[30] Mühlen HJ, van Heek KH, Jüntgen H. Kinetic studies of steam gasification of char in the presence of H_2, CO_2 and CO. Fuel 1985;64:591.
[31] Miura K, Hashimoto K, Sileston PL. Factors affecting the reactivity of coal chars during gasification, and indices representing reactivity. Fuel 1989;68:1461.
[32] Hurt RH, Lunden MM, Brehob EG, Maloney DJ. Statistical kinetics for pulverized coal combustion. Proc Combust Inst 1996;24:3169.
[33] Hurt RH, Davis KA, Yang NYC, Headley TR, Mitchell GD. Residual carbon from pulverised coal fired boilers: 2. Morphology and physicochemical properties. Fuel 1995; 74(9):1297–306.
[34] Hurt R, Sun J-K, Lunden M. A kinetic model of carbon burner in pulverized coal combustion. Combust Flame 1998; 113:181.
[35] Sun J-K, Hurt RH. A numerical study of the origin of unburned carbon. Ninth international conference on coal science, Essen, Germany, DGMK Tagungsberichte. 9703; 1997. p. 927–30.
[36] Hurt RH, Calo JM. Semi-global intrinsic kinetics for char combustion modeling. Combust Flame 2001;125:1138–49.
[37] Hurt RH. Development plan for CBK/gasification. Preliminary Report for Niksa Energy Associates, Belmont, CA; 2002.
[38] Blackwood JD, McGrory F. The carbon steam reaction at high pressure. Aust J Chem 1958;11:16.
[39] Blackwood JD, Ingeme AJ. Reaction of carbon with carbon dioxide at high pressure. Aust J Chem 1960;13:194.
[40] Liu G-S. Mathematical modeling of coal char reactivity in pressurized entrained flow gasifiers. PhD Thesis, Department of Chemical Engineering, University of Newcastle, Australia; 1999.
[41] Harris DJ, Patterson JH. Use of Australian bituminous coals in IGCC power generation technologies. Aust Inst Energy J 1995;13:22.
[42] Blackwood JD. The reaction of carbon with hydrogen at high pressure. Aust J Chem 1959;12:14.
[43] Tomita A, Mahajan OP, Walker Jr PL. Reactivity of heat-treated coals in hydrogen. Fuel 1977;56:490.
[44] Hong J-H. Modeling char oxidation as a function of pressure using an intrinsic Langmuir rate equation. PhD Dissertation, Department of Chemical Engineering, Brigham Young University, Utah; 2000.
[45] Satterfield CN. Mass transfer in heterogeneous catalysis. Cambridge, MA: MIT Press; 1970.
[46] Salatino P, Senneca O, Masi S. Assessment of thermodeactivation during gasification of a bituminous coal char. Energy Fuels 1999;13:1154–9.
[47] Essenhigh RH. Influence of initial particle density on the reaction model of porous carbon particles. Combust Flame 1994;99:269.
[48] Gavalas GR. A random capillary model with application to char gasification at chemical controlled rates. AIChE J 1980;26:557.
[49] Bhatia SK, Perlmutter DD. A random pore model for fluid–solid reactions: I. Isothermal, kinetic control. AIChE J 1980;26:379.
[50] Bhatia SK, Perlmutter DD. A random pore model for fluid–solid reactions: II. Diffusion and transport effects. AIChE J 1981;27:247.
[51] van Heek KH, Muehlen J-J. In: Lahaye, Ehrburger, editors. Fundamental issues in control of carbon gasification reactivity. Dordrecht: Kluwer; 1991.
[52] Lang T, Hurt RH. Char combustion reactivities for a suite of diverse solid fuels and char-forming organic model compounds. Proc Combust Inst 2002;29:423–31.
[53] Zolin A. Reactivity of solid fuels. PhD dissertation, Department of Chemical Engineering, Technical University of Denmark, Denmark; 2001.
[54] Kurose R, Ikeda M, Makino H. Combustion characteristics of high ash coal in a pulverized coal combustion. Fuel 2001;80: 1447–55.
[55] Penner SS. Chemistry problems in jet propulsion. New York: Pergamon Press; 1957.
[56] Niksa S, Liu G-S. Incorporating detailed reaction mechanisms into simulations of coal-nitrogen conversion in p.f. flames. Fuel 2002;81:2371–85.
[57] Niksa S, Liu G-S. Advanced CFD post-processing for p.f. flame structure and emissions. 28th International technical conference on coal utilization and fuel systems, Coal Technology Association, Clearwater, FL; March, 2003.
[58] Govind R, Shah J. Modeling and simulation of an entrained flow coal gasifier. AIChE J 1984;30:79.
[59] Niksa S, Cho S. Assigning meaningful stoichiometric ratios for pulverized coal flames. Proc Combust Inst 1998;27: 2905–13.
[60] Chen JC, Castagnoli C, Niksa S. Coal devolatilization during rapid transient heating. 2. Secondary pyrolysis. Energy Fuels 1992;6:264–71.